# The role of ABCC5 in the transport of inhibitory neuropeptides into vesicles




Matteo Broketa
Wolfson College
University of Oxford

Submitted in fulfilment of the requirements for the degree of Master of Science by Research in Physiology, Anatomy & Genetics

Trinity Term 2020

**Declaration**

I, Matteo Broketa, declare as follows:

1. That the work described in this thesis has not been submitted to the University of Oxford, or any other tertiary institution, for purposes of obtaining an academic qualification, whether by myself or any other party.
2. That I performed the entirety of the laboratory work presented as results in this thesis.
3. That the thesis I am submitting is entirely my own work except where otherwise indicated.

Matteo Broketa Date: 20 07 2020

# The role of ABCC5 in the transport of inhibitory neuropeptides into vesicles

Matteo Broketa

Wolfson College

Master of Science by Research in Physiology, Anatomy, and Genetics

Trinity Term 2020

## Abstract

ABCC5 is an ATPase dependent membrane transporter capable of transporting many structurally unrelated substrates such as glutamate conjugates and cyclic nucleotides. Previous work has found that high ABCC5 expression in human adipose tissue has been associated with an increased incidence of Type 2 diabetes mellitus. Global *Abcc5* knock-out mice had significant accumulation of the inhibitory neuropeptide *N*-acetylaspartylglutamate in their brains and had reduced adipose tissue depots, were more insulin sensitive and had raised post-prandial plasma levels of the incretin hormone GLP-1. We propose that ABCC5 may be involved with the loading of NAAG into synaptic-like microvesicles in gut endocrine cells and neurons. The work outlined here aimed to identify where ABCC5 is expressed in gut endocrine cells and to confirm the NAAG transporter activity of ABCC5. Through fixed cell immunolabelling and live cell dye staining, we show that ABCC5 is not expressed on the cell membrane of model enteroendocrine cells and has a punctate, intracellular expression pattern. We also adapted a method to isolate *ex vivo* synaptic vesicles from mouse brains and developed a vesicular transport assay with NAAG-$^{13}C_5$ substrate detection based on NMR spectroscopy. The preliminary data we have generated supports our hypothesis that ABCC5 is expressed intracellularly and participates in the loading of substrates in intracellular vesicle pools.

**Acknowledgements**

I must extend my utmost thanks to Prof Heidi de Wet for all her guidance and support that made all the work shown here possible. The other members of our lab, Ms Gosia Cyranka and Dr Natascia Vedovato, were also very supportive and generous in providing me with technical training and insight necessary to carry out this project. I am grateful to Prof Tim Claridge for his supervision and assistance in our NMR analysis. I would also like to thank the Micron Team for their excellent teaching and training in the practical use of microscopes.

**Declaration** ii

**Abstract** iii

**Acknowledgements** iv

**List of Figures** vii

**Abbreviations** viii

**1 Introduction**

**1.1 Insights into the function of ABCC5** 1

**1.2 GLP-1 in Type 2 Diabetes Mellitus** 1

**1.3 Early Connection between ABCC5 and T2DM** 4

**1.4 Work preceding this study:**

1.4.1 Expression of ABCC5 by intestinal endocrine cells 4

1.4.2 ABCC5 contributes to the secretion of GLP-1 by GLUTag cells 5

1.4.3 NAAG levels are altered by ABCC5 expression and effect GLP-1 secretion 5

1.4.4 *Abcc5* KO mice display a lack of pre-pulse inhibition 6

1.4.5 ABCC5 protein expression does not localize to the cell membrane 7

**1.5 RESEARCH HYPOTHESIS** 8

**2 Materials & Methods**

**2.1 Fixed Cell Immunofluorescence Labelling** 9

2.1.1 Cell Culture 9

2.1.2 Cell Fixation 9

2.1.3 Immunolabelling 10

2.1.4 Antibodies utilized in fixed cell immunofluorescence 10

2.1.5 Microscopy and Image Acquisition 11

**2.2 Isolation and culture of primary gut crypt cells** 12

**2.3 Live Cell Fluorescence Microscopy** 12

**2.4 Synaptic Vesicle Purification** 13

2.4.1 Animals 13
2.4.2 Vesicle Isolation from Mouse Brain 13
2.4.3 Dot-Immunobinding Assay 14
2.4.4 SDS-Page 14
2.4.5 Coomassie Stain 15
2.4.6 Western Blot 15
**2.5 NAAG Transport Assay** 15
2.5.1 Protein Quantification 15
2.5.2 Vesicular Transport assay 15
2.5.3 Vesicle Filtration 16
2.5.4 Detection of NAAG by NMR 16
**3 Results – Immunofluorescence Microscopy** 18
3.1 Introduction: Immunofluorescence labelling and Colocalization Analysis 18
3.2 Methods and Optimization 19
3.3 Results 24
3.4 Discussion 27
**4 Results – Live Cell Fluorescence Imaging** 29
4.1 Introduction: Fluorescein Diacetate 29
4.2 Results 30
4.3 Discussion 31
**5 Results –$^{13}$C-NAAG NMR Transport Assay** 34
5.1.1 Introduction: Membrane transporters and Vesicular transport assays 34
5.1.2 Nuclear Magnetic Resonance Spectroscopy 35
5.2 Transport Assay Development 37
5.3 NMR Results 41
5.4 Discussion 45
**6 General Discussion and Conclusion** 48
**References**

**List of Figures**


Figure 1.1 Summary of GLP-1 activity throughout the body

Figure 1.2 GLP-1 exocytosis is dependent on ABCC5 protein levels.

Figure 1.3 GLP-1 exocytosis is inhibited by NAAG

Figure 1.4 Pre-pulse inhibition (PPI) in Abcc5-/-mice and wild-type littermate controls

Figure 1.5 ABCC5 protein expression do not localize to the cell membrane

Figure 3.1 Diagram of indirect immunolabeling

Figure 3.2 Unoptimized immunolabelling for ABCC5

Figure 3.3 Optimization of ABCC5 immunofluorescence stain

Figure 3.4 Optimized ABCC5 immunofluorescence stain

Figure 3.5 Expression and localization of ABCC5 within NCI-H716 cells

Figure 3.6 Immunolabelling of ABCC5 and GLP-1 in primary gut crypts from mice

Figure 4.1 Molecular structures of fluorescein diacetate and fluorescein

Figure 4.2 Live cell imaging of NCI-H716 with FDA

Figure 5.1 Molecular structure of NAAG-$^{13}C_5$ and its associated NMR spectrum

Figure 5.2 Summary diagram of vesicle purification protocol

Figure 5.3 Western blots of vesicle purification preparation

Figure 5.4 Representative dot-blot assay of vesicle purification preparation

Figure 5.5 Summary diagram of adapted vesicle transport assay

Figure 5.6 Relative NAAG concentrations in vesicle transport assay and related spectra

Figure 6 Diagram of NAAG roles in the brain

**Abbreviations**

| | |
|---|---|
| ABCC5 | ATP-binding cassette subfamily C member 5 |
| ATP | Adenosine triphosphate |
| BMI | Body Mass Index |
| CFTR | Cystic fibrosis transmembrane conductance regulator |
| FACS | Fluorescence-activated cell sorting |
| FDA | Fluorescein diacetate |
| GABA | Gamma aminobutyric acid |
| GIP | Gastric inhibitory polypeptide |
| GLP-1 | Glucagon-like peptide 1 |
| GSIS | Glucose-stimulated insulin secretion |
| KO | Knock out |
| LAMP2 | Lysosome-associated membrane protein 2 |
| MRP | Multidrug resistance-associated protein |
| NAAG | *N*-acetylaspartylglutamate |
| $NAAG_2$ | *N*-acetylaspartylglutamylglutamate |
| NBF | Neutral buffered formalin |
| NEFA | Non-esterified fatty acid |
| NMR | Nuclear magnetic resonance |

| | |
|---|---|
| OE | Overexpression |
| PPI | Pre-pulse inhibition |
| RNA | Ribonucleic acid |
| RYGB | Roux-en-Y gastric bypass |
| siRNA | small interfering RNA |
| SLMV | Synaptic like microvesicle |
| SUR1/2 | Sulfonylurea receptor 1/2 |
| T2DM | Type 2 diabetes mellitus |
| TOMM20 | Translocase of outer mitochondrial membrane 20 |
| VGLUT1/2 | Vesicular glutamate transporter 1/2 |
| WT | Wild type |
| YFP | Yellow fluorescent protein |

# 1 Introduction

## 1.1 Insights into the function of ABCC5

ATP-binding cassette (ABC) transporters are a diverse family of membrane ATPase dependent transporters that translocate a large number of structurally unrelated compounds across extra- and intracellular membranes[1]. Eukaryotic ABC transporters predominantly function as exporters of compounds from the cytoplasm, with the main exceptions of the ABCC7(CFTR), which functions as an ion channel, and ABCC8(SUR1) and ABCC9(SUR2), which regulate ion channels. ABC transporters have also been reported in the literature as multidrug resistance-associated proteins (MRP) due to their ability to export exogenous anticancer or antiviral drugs and roles in multi-drug resistance, namely ABCB1, ABCC1, and ABCG2[2].

ABCC5 was an "orphan" ABC transporter known to be highly expressed in neurons, glial cells, and the blood brain barrier, but with little understanding regarding its endogenous substrates and function. ABCC5 has previously been identified as an exporter of glutamate conjugates and analogues [3] using untargeted metabolomics screens on *Abcc5-/-* mice. Glutamate conjugates were accumulated in multiple tissues and particularly the brain, with the inhibitory neurotransmitters *N*-acetylaspartyl glutamate (NAAG) and *N*-acetylaspartyldiglutamate ($NAAG_2$) being the most abundant within the *Abcc5-/-* mouse brains. NAAG functions as an antagonist toward glutamatergic activation and is believed to be neuroprotective by preventing excitotoxicity[4-6].

## 1.2 GLP-1 in Type 2 Diabetes Mellitus

Type 2 diabetes mellitus (T2DM) is a disease primarily characterized by chronic hyperglycaemia that is the result of insufficient insulin release by pancreatic islet β-cells. The demand for insulin secretion is determined by a dynamic relationship between the insulin sensitivity of peripheral tissues and glucose homeostasis [7]. The most prevalent and critical factor affecting these

parameters is obesity, which has been associated with increased insulin resistance and an increase in circulating levels of non-esterified fatty acids (NEFA) and pro-inflammatory cytokines [8]. However, the majority of insulin-resistant, obese individuals do no develop hyperglycaemia; β-cells demonstrate sufficiently increased insulin release to compensate for the reduced efficacy of insulin in target tissues, thereby maintaining normoglycemia [9]. For insulin resistance and obesity to result in T2DM, islet β-cell function is compromised and characterized by an inability to fully compensate for reduced insulin sensitivity.

Insufficient insulin release has been shown to not be the result of a lack of insulin content within β-cells of individuals with type 2 diabetes [10]. Additionally, the approximate 50% loss of β-cell mass observed in T2DM [11] is unlikely to fully cause the decrease in insulin release, as β-cell function at the time of diagnosis is already a quarter of its normal functional capacity [12]. Notwithstanding, changes to glucose-stimulated insulin secretion (GSIS) are a strong putative source of insufficient insulin release, and is evidenced by defective GSIS in islets from T2DM donors compared to non-diabetic donors [13] as well as the disruption of GSIS by NEFAs [14, 15], which are frequently elevated in T2DM patients.

A key factor of β-cell function and GSIS is the effect of incretin hormones released by entero-endocrine cells, namely glucagon-like peptide 1 (GLP-1) and gastric inhibitory peptide (GIP). GLP-1 and GIP are released from enteroendocrine cells in response to oral glucose administration, and are well established to potentiate insulin release by β-cells and improve glucose tolerance [16]. Interestingly, GLP-1 levels in the plasma of obese individuals were unchanged in obese subjects and even decreased in morbidly obese subjects, yet post prandial insulin release was increased compared to lean subjects, which suggests β-cells may become more sensitive to GLP-1 during obesity [17].

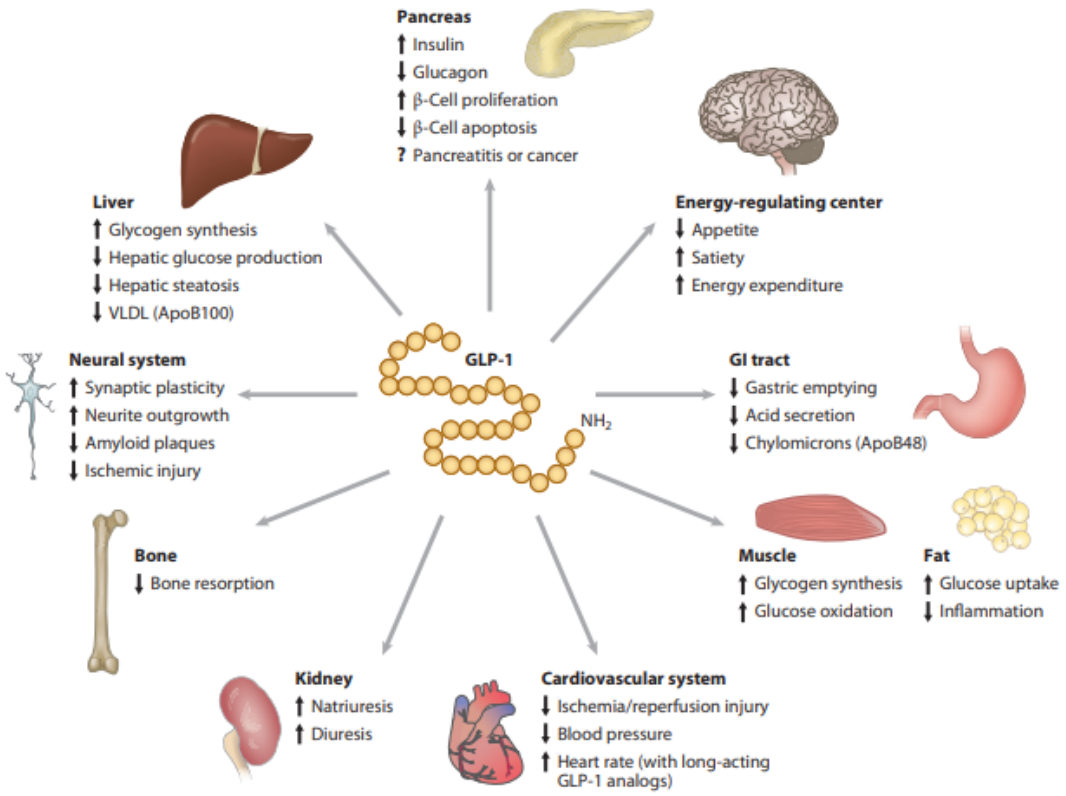



**Figure 1.1** Summary of GLP-1 activity throughout the body. Adapted from Cho, Fujita, and Kieffer (2014), Glucagon-Like Peptide-1: Glucose Homeostasis and Beyond. [18] Annual Review of Physiology, 2014. **76**(1): p. 535-559.

The capacity of GLP-1 to potentiate insulin release and manage T2DM has been exploited with outstanding success through pharmacological and surgical interventions. Direct infusion of GLP-1 has been shown to have an insulinotropic effect, slow gastric emptying, and decrease plasma glucagon concentrations [19, 20]. Additionally, degradation-resistant GLP-1 receptor agonists and dipeptidyl peptidase-4 (GLP-1 degrading enzyme) inhibitors have been developed and prescribed broadly to T2DM patients with great success, with lower rates of hypoglycaemia than sulfonylureas due to their glucose-dependent activity [21]. Another clinical option often pursued by highly obese individuals is bariatric surgery, with Roux-en-Y gastric bypass (RYGB) and vertical sleeve gastrectomy being the most common [22, 23]. Bariatric surgery is currently the most effective treatment for lowering BMI and aiding in remission from T2DM. Substantial evidence has been gathered showing significantly elevated postprandial GLP-1 following RYGB is associated with increased satiety and decreased fasting glucose and insulin levels [24-26].

### 1.3 Early connection between ABCC5 and T2DM

The first demonstration of ABCC5 participating in metabolism, obesity, and T2DM came from a candidate gene study on T2DM patients, which identified *ABCC5* and particularly its increased expression to confer an increased risk of developing T2DM with age [27]. An *ABCC5* variant associated with increased ABCC5 expression in adipose tissue was shown to be positively correlated with T2DM and insulin resistance. Additionally, higher *ABCC5* expression levels were associated with increased visceral adipose accumulation, an almost four times increased risk of developing T2DM, as well as decreased peripheral insulin sensitivity within the non-diabetic cohort. The range and significance of the associations between ABCC5 and T2DM demonstrated by this genetic study strongly suggested that the expression and/or activity of ABCC5 may contribute to the development of T2DM.

### 1.4 Work preceding this study:

#### 1.4.1 Expression of ABCC5 by intestinal endocrine cells

RNA sequencing of hormone secreting cells from the mouse gut has previously been performed by Prof Fiona Gribble and Dr Frank Reimann (University of Cambridge, UK)[28, 29]. Cells were FACS sorted from intestinal sections of NeuroD1-CrexRosa26EYFP and GLU-Venus mice, which have been made to express yellow fluorescent protein (YFP) in enteroendocrine cells and GLP-1-secreting L-cells (enteroendocrine cell subtype), respectively. Total RNA was sequenced from isolated YFP positive and negative cell populations and then aligned against the mouse genome. Expression of *Abcc5* was shown to be significantly increased in duodenal enteroendocrine cells ($p=0.001$) and in ileal L cells ($p=0.019$) relative to nonendocrine cells ($YFP^-$). GLUTag cells, a model mouse L-cell line that secretes GLP-1 in response to nutrient stimuli [30, 31], were also RNA sequenced by our lab and found to contain *Abcc5* mRNA levels comparable to those observed in cells isolated from mouse intestines earlier [29].

### 1.4.2 ABCC5 contributes to the secretion of GLP-1 by GLUTag cells

Our lab has previously used GLUTag cells to demonstrate a relationship between ABCC5 expression and GLP-1 secretion by intestinal endocrine cells (Figure 1.2 A & B). Suppression of *Abcc5* gene expression by siRNA knockdown resulted in an approximately 60% increase in GLP-1 secretion. Conversely, overexpression of *ABCC5* by a recombinant plasmid resulted in the attenuation of GLP-1 secretion to less than that observed in GLUTag cells with normal *ABCC5* expression. The inverse relationship between *ABCC5* expression and GLP-1 exocytosis levels characterized by these results strongly suggested that ABCC5 plays an inhibitory role in GLP-1 secretion in response to stimulation by glucose.

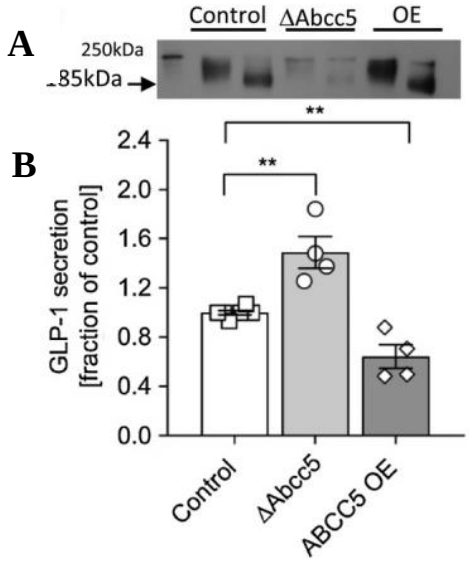



**Figure 1.2** GLP-1 exocytosis is dependent on ABCC5 protein levels. (**A)** Western Blot analysis of WT GLUTag cells (lanes 1,2), GLUTag cells with siRNA knockdown of *ABCC5* (lanes 3,4), and overexpressed (OE) ABCC5 (lanes 5,6). Lanes 1,3,5: unheated samples; lanes 2,4,6: heated samples. (**B**) GLP-1 secretion following a 2-hour incubation in 5.6mM glucose (n=4) as determined by ELISA (Cisbio); presented as fraction of GLP-1 secreted by WT GLUTag in 5.6mM glucose. *shown as mean ± SEM, analysed by an unpaired Welch's unequal variances t test; **$P \leq 0.01$.* [29] Obesity (Silver Spring, Md.), 2019. **27**(8): p. 1292-1304.

### 1.4.3 NAAG levels are altered by ABCC5 expression and effect GLP-1 secretion

Jansen *et al* [3] have previously reported that the knockdown of *Abcc5* results in the accumulation of NAAG within the mouse brain and other tissues. Using comparative metabolomics, our lab confirmed the inverse relationship between *ABCC5* expression and NAAG levels within GLUTag cells (Figure 1.3A). Overexpression of *ABCC5* was associated with a decrease in intracellular

NAAG levels relative to mock transfected GLUTag cells. Furthermore, our lab sought to investigate the potential participation of NAAG in the changes to GLP-1 secretion observed from altered *Abcc5* expression. Exogenous NAAG was administered to GLUTag cells as well as *Abcc5* KO *ex vivo* mouse gut crypt primary cell lines and in both cases inhibited GLP-1 secretion (Figure 1.3B/C).

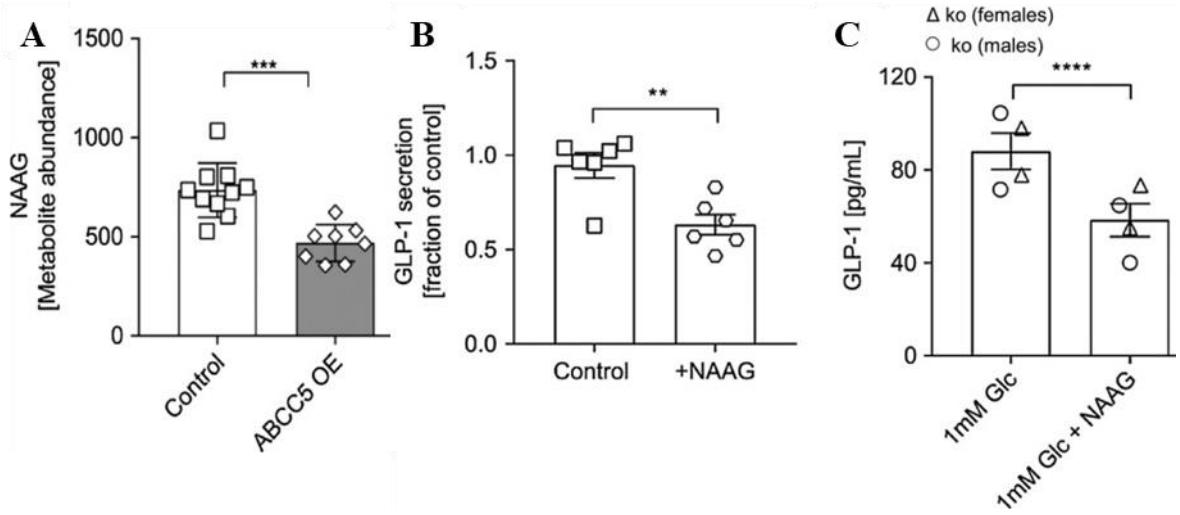



**Figure 1.3** GLP-1 exocytosis is inhibited by NAAG (**A**) Overexpression of *ABCC5* decreased intracellular NAAG in GLUTag cells relative to controls (n=8), in arbitrary units (**B**) Inhibition of GLP-1 secretion by exogenous NAAG added to GLUTag cells (n=6) or (**C**) ex vivo gut crypt primary small intestine cultures of *Abcc5*$^{-/-}$ mice ($n = 4$). Data shown as mean ± SEM and **A** & **B** were analysed by an unpaired two-tailed Student *t* test; **C** analysed by an unpaired Welch's unequal variances *t* test. $^{**}P \leq 0.01$; $^{***}P \leq 0.001$; $^{****}P \leq 0.0001$; [29]

### 1.4.4 *Abcc5* KO mice display a lack of pre-pulse inhibition

In addition to their metabolic phenotype, *Abcc5* KO mice also display a distinct schizophrenic behavioural phenotype. Pre pulse inhibition (PPI) of the mammalian startle response is a behavioural phenomenon that is often disrupted in schizophrenia, and measurement of PPI is an effective biomarker for schizophrenia[32] (Fig1.4A). Abcc5 KO mice showed a significant impairment of their PPI and had increased startle responses (Fig 1.4B), strongly suggesting the mice are schizophrenic. Hypofunction of the NMDA receptor is a major contributor to schizophrenia development, and NAAG has been previously characterized as both an inhibitor of presynaptic glutamate release and an NMDAR antagonist[33]. The emergence of schizophrenia in *Abcc5* KO mice suggests that ABCC5 may have a role in neural NAAG transport and signalling.

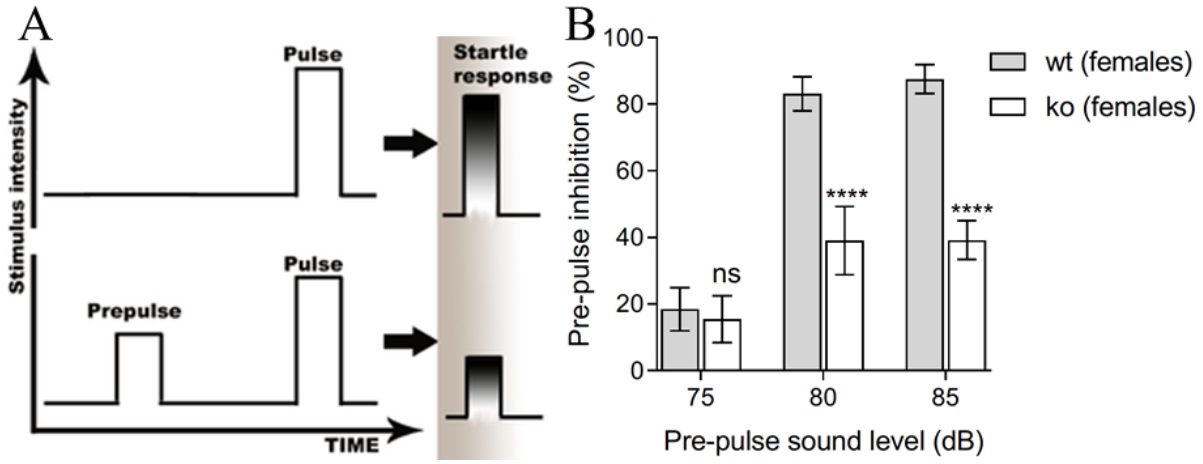



**Figure 1.4 -** Pre-pulse inhibition (PPI) in Abcc5-/-mice and WT littermate controls. (**A**) principle of PPI – weaker pre-pulse (58dB or 65dB) followed by the startle stimulus (120dB) lowers the reaction to the startle stimulus. (**B**) Mean % PPI ± SEM in 15 weeks old females, WT, Abcc5-/- Data were analyzed using an unpaired two-tailed Student's t-test; ****P≤ 0.0001.

### 1.4.5 ABCC5 protein expression does not localize to the cell membrane

Preliminary immunofluorescence microscopy images found ABCC5 to be expressed intracellularly in both GLUTag cells and L-cells from GLU-Venus mouse ileum (Fig1.5A/B), in contrast to many prior observations of ABC transporters localizing to the cell membrane [34-36]. Additionally, within GLUTag cells ABCC5 did not appear to colocalize with the GLP-1 containing secretory granules.

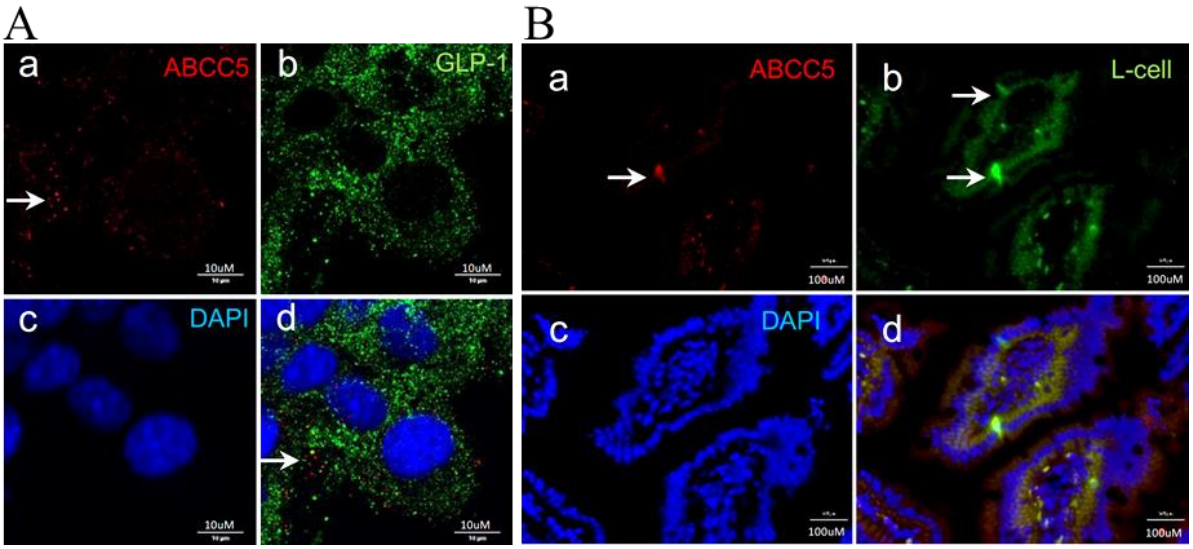



**Figure 1.5** (**A**) ABCC5 protein expression (red) in GLUTag cells shows punctate, intracellular localization and did not co-localize with GLP-1 containing vesicles (green). Nuclei are visualized by DAPI (blue) (**B**) ABCC5 protein expression (a, red) is observed in GLP-1 expressing enteroendocrine cells (b, green) in GLUVenus mouse ileum. Nuclei were visualized by DAPI (blue).[29]

## 1.5 Research Hypothesis

Given the inverse relationship between ABCC5 protein expression and GLP-1 release as well as the known function of ABCC5 as an exporter, we hypothesize that ABCC5 may participate in the transport of inhibitory neuropeptides within gut endocrine cells. Furthermore, due to the significantly increased abundance of NAAG in *Abcc*5 KO mice, we hypothesize that ABCC5 is involved specifically in the transport of the inhibitory neuropeptide *N*-acetylaspartylglutamate (NAAG).

Additionally, as previous work has shown ABCC5 to be expressed intracellularly within gut endocrine cells and not at the cell membrane, we hypothesize that ABCC5 is involved in the loading of inhibitory neuropeptides, particularly of NAAG, into synaptic-like microvesicles (SLMVs) in both gut endocrine cells and neurons.

## 1.6 Aims & Objectives

The aims of this thesis are to deepen our mechanistic understanding of how ABCC5, particularly through its transport function, influences the release of GLP-1 and ascertain if ABCC5 has a role in the brain. I have worked to address these aims by:

- Identifying where ABCC5 is expressed in human model L cells and *ex vivo* mouse gut crypts using immunofluorescence microscopy and dyes, to eliminate the possibility of ABCC5 cell surface expression.
- Confirming whether ABCC5 has NAAG transport activity in synaptic vesicles isolated from mouse brains.

# 2 Materials & Methods

## 2.1 Fixed cell Immunofluorescence Labelling

### 2.1.1 Cell Culture

GLUTag cells, a mouse model L cell line, were grown in T75 $cm^2$ flasks coated with 0.8% Matrigel® matrix solution. Cells were incubated at 37°C with 5% $CO_2$. Cells were cultured in low glucose Dulbecco's Modified Eagles Medium (DMEM) [Gibco, 31885] supplemented with 10% Heat-Inactivated Fetal Bovine Serum (HI-FBS) [Sigma, F9665]. Media was replaced every 2-3 days. Cells were grown to 80% confluency and then split (every 4-5 days). To split, cells were washed with pre-warmed Dulbecco's Phosphate Buffered Saline (PBS) [Gibco, 14190-250], detached by addition of EDTA/Trypsin [Gibco, 25300-054] incubated for 3 mins at 37°C. Trypsin was inactivated by the addition of DMEM containing HI-FBS and the cells resuspended at a concentration of $1x10^6$ cells per ml. $1x10^6$ cells were reseeded per fresh coated flask.

NCI-H716 cells , a human model L cell line, were grown in suspension in uncoated T75 $cm^2$ flasks. Cells were incubated at 37°C with 5% $CO_2$. Cells were cultured in low glucose Roswell Park Memorial Institute (RPMI) 1640 Medium [Gibco, 11875093] supplemented with 10% Fetal Bovine Serum (FBS) [Sigma, F7524]. Cells were grown to 70% confluency and then split (every 3-4 days). To split, cells were pelleted by centrifugation at 300*g* for 3 minutes and resuspended at a concentration of $1x10^6$ cells per ml. $1x10^6$ cells were reseeded per fresh flask.

### 2.1.2 Cell Fixation and Permeabilization

Prior to fixation, cells were seeded at a density of $4x10^5$ cells per well in an 8-well Nunc Lab-Tek II Chamber Slide System [Thermo Fischer, 154534] or a µ-Slide 8 Well glass bottom chambered coverslip [Ibidi, 80827]**,** coated with 1-2% Matrigel® matrix solution. Cells were cultured as described above for 24 hours. At the start of fixation, culture media was removed, and wells were washed four times with PBS for 5 minutes. Where methanol fixation is indicated, cells were fixed using 100% methanol at -20°C for 5 minutes. Where Neutral Buffered Formalin (NBF) fixation is

indicated, samples were fixed using 10% NBF for 10 minutes at room temperature. Following fixation, wells were washed three times with PBS for 5 minutes. Following NBF fixation, samples were also permeabilised with 0.25% Triton X-100 [Sigma, X100] in PBS for 10 minutes, which was followed by washing three times with PBS for 5 minutes.

### 2.1.3 Immunolabelling

Cells were blocked using SuperBlock™ (TBS) blocking buffer [ThermoFisher, 37581] for 1 hour at room temperature. Cells were incubated with primary antibody for 1 hour at 37°C in a humid chamber for methanol fixed samples, or overnight at 4°C for NBF fixed samples. Primary antibody solution was removed, and wells were washed four times with PBS for 5 minutes. Cells were incubated with secondary antibody for one hour at room temperature in a dark, humid chamber and on a three-dimensional orbit rocker. Secondary antibody solution was removed, and wells were washed four times with PBS for 5 minutes. DAPI stain [Sigma, D9542] in a 1:1000 dilution was added for 10 mins at room temperature in a dark chamber and wells were washed two times with PBS for 5 minutes. Primary and secondary antibodies and counterstain were diluted using SuperBlock™ blocking buffer. Prior to mounting, the media chamber was removed, and excess glue removed using a scalpel. Slides were mounted using ProLong™ Gold antifade mountant [ThermoFisher, P36930], covered with an appropriately sized cover slip, and cured for at least 48 hours in the dark at room temperature prior to imaging.

### 2.1.4 Antibodies utilized in fixed cell immunofluorescence

| Target | Manufacturer and Catalogue Number | Ab species, clonality, and antigen species | Dilution Used | Intended Cellular Target |
|---|---|---|---|---|
| ABCC5/MRP5 | Santa Cruz Biotechnology (H-100) sc-20769 | Rabbit Polyclonal Anti-human | 1:50 | To be investigated |
| | Santa Cruz Biotechnology (E-10) sc-376965 | Mouse Monoclonal Anti-human | 1:50 | To be investigated |
| | Santa Cruz Biotechnology (P-20): sc-5781 | Goat Monoclonal Anti-human | 1:50 | To be investigated |

| | | | | |
|---|---|---|---|---|
| GLP-1 | LSBio LS-C490378 | Rabbit Polyclonal Anti-human | 1:500 | GLP-1 secretory granules |
| VGLUT2 | Invitrogen 42-7800 | Rabbit Polyclonal Anti-mouse | 1:300 | GLP-1 secretory granules |
| VGLUT1 | Sigma HPA063679 | Rabbit Polyclonal Anti-human | 1:500 | Synaptic-like vesicles |
| Synaptophysin | Sino Biological 100136-T32 | Rabbit Polyclonal Anti-human | 1:200 | Synaptic-like microvesicles |
| LAMP2 | Sigma L0668 | Rabbit Polyclonal Anti-mouse | 1:200 | Lysosomes |
| TOMM20 | Abcam ab78547 | Rabbit Polyclonal Anti-human | 1:100 | Mitochondria |
| **Secondary Antibodies** | | | | |
| Mouse IgG | Abcam ab175700 | Donkey Polyclonal Alexa Fluor® 568 | 1:1000 | |
| Rabbit IgG | Abcam ab175692 | Donkey Polyclonal Alexa Fluor® 568 | 1:1000 | |
| | Abcam ab170053 | Donkey Polyclonal Alexa Fluor® 488 | 1:1000 | |
| | ThermoFischer SA1-200 | Donkey Polyclonal HRP | 1:10000 | |
| Goat IgG | Invitrogen A11057 | Donkey Polyclonal Alexa Fluor® 568 | 1:1000 | |
| | Promega V8051 | Donkey Polyclonal HRP | 1:10000 | |

### 2.1.5 Microscopy and Image Acquisition

All samples imaged contained a no antibody (nAb) control to check for autofluorescence, as well as no primary antibody controls (npAb) for each primary to assess secondary antibody specificity. Preliminary optimization images were generated using a Zeiss Axioplan2 upright widefield microscope and Zeiss AxioCam HRm camera, illuminated by a Zeiss HXP 120C lamp, with a 60x 1.4NA objective lens. Images for use in colocalization analysis were acquired using a Deltavision

Elite inverted widefield microscope with a CCD camera and a 100x 1.4NA objective lens. Prior to imaging, alignment and even illumination of the light source with the sample was confirmed. 1.5 coverslips (0.17mm) were used as necessary for the objectives selected. All image data was stored and transferred in the file formats of the microscope systems utilized.

### 2.2 Isolation and culture of primary gut crypt cells

Training and assistance with crypt isolation provided by Ms Gosia Cyranka. To obtain primary gut cells *Abcc5*$^{-/-}$ and littermate wildtype mice, we dissect the jejunem and ileum of the murine small intestine. The intestine is then cut longitudinally, thoroughly rinsed with cold PBS, and finely diced with a scalpel. The tissue pieces were then repeatedly digested with collagenase for a minimum of 3 cycles. Each cycle began with adding 8ml of collagenase medium (Sigma, C9407-10MG)[29] and incubating for 5-10 minutes at 37°C. After thoroughly shaking and allowing tissue to settle, the supernatant was collected and assessed for crypt purity. Settled tissue was then resuspended in 8ml of collagenase medium and the cycle was repeated. Fractions with high crypt enrichment were collected into 15ml tubs and centrifuged at 300g for 5 minutes. The pelleted crypts were resuspended in the growth media: DMEM (Sigma, D6546-500ML) supplemented with 100U/mL penicillin and 100µg/mL streptomycin (Gibco, 15140122), 10% FBS (Sigma), 2mM Glutamine, 10uM ROCK inhibitor (Y27632), and passed through a 100µm strainer. Crypts were plated onto Matrigel coated chamber slides containing growth media and incubated at 37°C, 5% $CO_2$ for at least 24 hours prior to NBF fixation.[37]

### 2.3 Live Cell Fluorescence Microscopy

NCI-H716 cells were cultured as described above, then seeded at a density of 4E5 cells per well in an 8-well Nunc Lab-Tek II Chamber Slide coated with 1-2% Matrigel® matrix solution. Cells were incubated for at least 24 hours. Culture media was removed, and wells were washed twice with PBS. 25µM FDA-RPMI medium with no FBS was then added to each well and incubated at 37C for 5 minutes. Staining solution was removed from wells, washed twice with PBS, and afterward

PBS was again added to the wells. Slides were then returned to the incubator for the length of time indicated prior to imaging. Cells were imaged using an EVOS AMF4300 microscope.

## 2.4 Synaptic Vesicle Purification

### 2.4.1 Animals

*Abcc5* knockout mice were generated by MRC Harwell using CRISPR/Cas9 technology to create a 372nt deletion of Exon ENSMUSE00001236135 in murine embryos from a C57BL/6NTac background strain. All procedures were performed in accordance with the Animal (Scientific Procedures) Act 1986, UK, Amendment Regulations 2012 (SI 4 2012/3039).

### 2.4.2 Vesicle Isolation from Mouse Brain

Protocol based on Ahmed *et al*[38], with adjustments for the use of frozen mouse brains. Centrifugation at 1,000*g* was done using an Allegra 6KR centrifuge [Beckman Coulter] and centrifugations between 15,000*g* and 165,000*g* were performed with an Optima L-100 XP Ultracentrifuge [Beckman Coulter] and an SW 32 Ti rotor [Beckman Coulter]. Samples for ultracentrifugation were placed into Ultra-Clear centrifuge tubes [Beckman Instruments, 344058]. Appropriate r.p.m and spin time for our centrifuge and rotor were converted from those published by Ahmed *et al*[38] using the Beckman Coulter online rotor calculator [https://www.mybeckman.uk/centrifuges/rotors/calculator]. Snap frozen brains [extracted and frozen by Dr Natascia Vedovato] were quickly warmed by adding 1ml of room temperature homogenization buffer or HomBuff [320mM sucrose, 4mM NaOH-HEPES (HEPES buffer pH adjusted to pH 7.4 using 3M NaOH)] and dipping into a 37°C water bath. All further steps were performed at +4°C on ice. Pieces of brain were homogenized in HomBuff and cOmplete protease inhibitor cocktail [Sigma, 04-693-116-001] with a dounce homogenizer. The homogenization mixture was centrifuged at 1,000*g* (2,500 r.p.m) for 10 minutes at +4°C, the supernatant (SN1) was collected, and the pellet discarded. The SN1 was centrifuged at 15,000*g* (9,000 r.p.m) for 15 minutes at +4°C and the supernatant (SN2) was collected. The pellet (P2) was resuspended in

HomBuff, while avoiding the brown bottom part of the pellet that consists primarily of mitochondria. The P2 was added to a dounce homogenizer with double distilled $H_2O$ ($ddH_2O$) and homogenized with 10 strokes, followed immediately by the addition of NaOH-HEPES and cOmplete protease inhibitor cocktail. The osmotic lysate from the P2 was centrifuged at 17,000*g* (10,000 r.p.m) for 15 minutes at +4°C, and the supernatant (LS1) was collected. The LS1 and S2 were combined and the LS1/S2 mixture was centrifuged at 48,000*g* (17,000 r.p.m) for 25 min at 4 °C. The supernatant (CS1) was collected and drawn into a syringe through a 19-gauge needle. The CS1 was then expelled through a 26-gauge needle on top of a 0.7 M sucrose cushion. The sucrose cushion was centrifuged at 165,000*g* (31,000 r.p.m) for 100 minutes at +4°C. 20 fractions of 1,800µl as well as the pellet were collected from the centrifuged sucrose cushion, starting from the top of the gradient. Collected fractions were stored at -80°C. During the procedure, 50µl aliquots were taken from the homogenization mixture, the pellets from centrifugation at 1,000*g*, 15,000*g*, 17,000*g*, and 48,000*g*, and the supernatant from centrifugation at 48,000*g*. Several preparations were performed in parallel with Dr Vedovato.

### 2.4.3 Dot-Immunobinding Assay

Polyvinylidene Difluoride (PVDF) membrane (0.2 µm pore size) [BioRad, 1620177] was primed using 100% methanol for 3 minutes, then washed in $ddH_2O$ and placed in Tris-Buffered Saline (TBS) -0.1% Tween (TBS-T) for 5 minutes. After drying the primed PVDF, a drop of each fraction was added to the membrane. Membranes were blocked with 5% milk - TBS-T solution for 1 hour at room temperature and then washed two times in TBS-T for 2 minutes. Membranes were incubated with anti-synaptophysin rabbit polyclonal antibody [SB, 100136-T32] at a 1:500 dilution in 0.5% milk – TBS-T solution for 30 minutes on a tube rotator [VWR], and then washed two times in TBS-T for 2 minutes. Membranes were incubated with secondary HRP-conjugated antibody diluted in 2% milk – TBS-T solution for 30 minutes on a tube rotator [VWR]. Membranes were thoroughly washed for 10 minutes and then another three 5-minute washes. Enhanced

chemiluminescence (ECL) solution [Fischer, 45-000-875] was applied to the whole of the membrane and incubated for 5 minutes in the dark.

#### 2.4.4 SDS-PAGE

35ul of sample mixed with Lithium Dodecyl Sulfate (LDS) sample buffer [Thermo Fisher Scientific] and Dithiothreitol (DTT) [Sigma Aldrich] was loaded to each well of a hand-cast 12% polyacrylamide gel, with 5% stacking gel. Gels were run for 1 hour at 150V. Gels were run in duplicate to enable one gel to be used for total protein visualization and one to be used for immunoblotting.

#### 2.4.5 Coomassie stain

The duplicate gel run was stained with Coomassie Brilliant Blue R250 staining solution [BioRad] for 3 hours with gentle agitation. The stained gel was then destained overnight with Coomassie Brilliant Blue R-250 destaining solution [BioRad] also under gentle agitation. Gel and film images were captured using the Epson Perfection 3490 scanner.

#### 2.4.6 Western Blot

A wet tank transfer was performed. PVDF membrane was primed as described in the dot-immunobinding assay. The transfer sandwich was assembled, and transfer was performed on ice for 3 hours at 300mA. After transfer, the membrane was washed twice for 5 mins in TBS-T with agitation. Membrane was blocked using 5% milk TBS-T for 1 hour at room temperature, followed by incubation with either anti-synaptophysin(1:500) or anti-ABCC5(sc-5781, 1:200) primary antibody diluted in 5% milk TBS-T overnight at +4°C. Membranes were washed 3 times using TBS-T and agitation for 15 minutes prior to incubation with Horseradish Peroxidase (HRP)-conjugated secondary antibody diluted in 5% milk TBS-T for 1 hour at room temperature. A final step of three 15-minute washes with TBS-T was performed to remove unbound secondary antibodies. ECL was applied to the whole of the membrane and incubated for 5 minutes in the dark.

### 2.5 NAAG Transport Assay

### 2.5.1 Protein quantification

Total protein concentration for each purified vesicle sample was quantified by the Pierce Bicinchoninic Acid Assay (BCA) Kit [Thermo Fisher Scientific, 23225] according to the manufacturer's instructions.

### 2.5.2 Vesicular Transport Assay

Protocol was adapted from Hell *et al* [38, 39]. Synaptophysin+ vesicle fractions from vesicle purification were combined and centrifuged at 275,000 g (40,000 r.p.m) for 3h 45 m using an SW 41Ti rotor [Beckman Coulter] to collect the vesicles into a pellet. Pellets were resuspended in 300µl of transport assay buffer (320mM sucrose, 4mM KCl, 4mM MgSO4, 10mM HEPES-KOH) and their total protein concentration was quantified as described. Protein was adjusted to 1.2 mg/ml if necessary. Prepared on ice, 125µl of vesicle suspension was combined with 20µl of 32mM NAAG-$^{13}C_5$ [Sigma Aldrich, 901017], 55µl of transport assay buffer, and 1.5µl of 300mM ATP (2mM final concentration) if necessary. Samples were then placed onto a heat block at 37°C. After 20 minutes, samples were replaced onto ice.

### 2.5.3 Vesicle Filtration

245µl of transport assay buffer was added to vesicle samples following the transport assay. Samples were drawn through 19-gauge needle into a 1ml syringe and then loaded into another 1ml syringe with a 0.22µm 4mm PVDF syringe filter on its tip. Samples were filtered completely and the "assay buffer filtrate" was collected. The syringe filter was then cut open using a scalpel and the filter membrane was carefully transferred into 430µl of 80% methanol. The "vesicle eluate" sample was then mildly vortexed for 5 minutes to separate vesicles and contents from the filter. The filter was then removed, and samples were stored at 4°C prior to measurement.

### 2.5.4 Detection of NAAG by NMR

Following sample preparation, 5 µl of 1M maleic acid [Supelco, 92816] was added to each sample to serve as an internal reference compound. Samples were then delivered to Prof Tim Claridge

[NMR Facility Director for Organic Chemistry and Chemical Biology, CRL Oxford] for measurement using a Bruker AVII 500 NMR spectrometer with a dual $^{1}H/^{13}C$ cryoprobe regulated at 25 $C^{o}$. All proton-decoupled 13C NMR data were acquired using identical parameters: number of scans (NS) =3072, spectral width (SW) = 250 ppm centered at 100 ppm, AQ = 1 s. MestReNova 14.1.2 analysis software was used for all spectrum processing and measurement. Apodization, phase correction, baseline correction, and zero filling [256K] was applied to all spectra prior to peak integration.

# 3 Results: Immunofluorescence Microscopy

## 3.1.1 Introduction: Immunofluorescence labelling and Multi-labelling

Fluorescence microscopy is a valuable tool in biology that allows for the visualization and quantification of specific cellular contents and structures. A common application of fluorescence microscopy examines the spatial distributions of two or more fluorescently labelled molecules to make inferences regarding their potential functional association within the same structures or molecular pathways. This technique allows for a molecule of unknown function to be putatively associated with the function and/or behaviour of another molecule or structure given the two have sufficient spatial overlap or colocalization. While a weak indicator of physiology, the demonstration of spatial association or conversely non-association can be invaluable to inform the planning of more powerful assays to determine function or imaging techniques able to visualize physical apposition, such as electron microscopy or fluorescence resonance energy transfer.

To utilize colocalization analysis by fluorescence microscopy to address our research hypothesis, we must select proteins known to localize within synaptic-like microvesicles as well as other vesicular pools. Given the large role of GLP-1 secretion in intestinal L-cell physiology and the changes to secretion observed during altered ABCC5 expression, GLP-1 is a polypeptide of major interest. Additionally, work by Uehara *et al* [40] demonstrated that GLP-1 is colocalized with the vesicular glutamate transporter 2 (VGLUT2) within intestinal L cells. VGLUT2 can therefore serve as a vesicle membrane marker of GLP-1 containing secretory granules to compare against the distribution of ABCC5. Uehara *et al* also show that VGLUT2 transports glutamate into GLP-1-secretory granules and that glutamate is coreleased with GLP-1 following nutrient stimulation of intestinal L cells. These findings designate these vesicles, GLP-1, and VGLUT2 as likely being part of a glutamatergic secretory pathway of intestinal L cells. Given our current hypothesis that ABCC5 transports and mediates vesicular loading of NAAG, which acts antagonistically to glutamatergic activation, we would expect ABCC5 to not be present on/within GLP-1/VGLUT2-

bearing vesicles. However, the full behaviour of ABCC5 is still unknown and the corelease of opposing neurotransmitters (glutamate + GABA) has been previously reported in other contexts[41], so the assumption of a lack of colocalization should not be made during analysis.

Although VGLUT1 was not detected within GLUTag cells by Uehara *et al* [40], RNA sequencing of the human NCI-H716 enteroendocrine cell line found low level expression of VGLUT1 transcripts[42]. Furthermore, considering the general importance of VGLUT1 in glutamatergic signalling [43, 44], VGLUT1 will also be an important target for colocalization analysis with ABCC5.

An important general marker for synaptic vesicles or similar secretory vesicles is synaptophysin. Despite having an unclear role and an apparent nonessential function within vesicles, synaptophysin's near ubiquitous expression in synaptic vesicles has designated it as a critical marker of synaptic transmission[45]. Colocalization of ABCC5 with synaptophysin would strongly suggest vesicular expression of ABCC5 and greatly increase our confidence in its potential role as a vesicular transporter. Finally, given the relative uncertainty regarding ABCC5 function, it will be valuable to assess the colocalization of ABCC5 with other major organelle markers for potential associations outside of our hypotheses. Lysosomes have previously been associated with the ABCA3 transporter[46], and so we will also investigate LAMP2 as a lysosomal marker[47]. From these general targets as well as the hypothesis-specific targets, colocalization analysis via immunofluorescence microscopy will be highly informative as to the spatial distribution of ABCC5 within cells and its potential intracellular role.

### 3.2 **Methods and Optimization**

Numerous methods have now been developed to link a molecule of interest with a fluorophore, each differently optimised for specificity, signal to noise ratio, ease of use, and application. The fluorescence microscopy carried out in this work utilized indirect immunofluorescence labelling to target molecules for imaging. Immunolabelling is a technique based upon the capacity for

antibodies to specifically target molecular structures of interest and the attachment of a fluorescent molecule to that antibody; fluorescence is thereby transitively attributed to the molecule or structure of interest via the antibody. As a cost-saving and applicability optimisation, the fluorescent molecule can be indirectly attached to the molecule of interest-recognizing "primary" antibody through a "secondary" antibody specific to the species of animal from which the primary antibody was derived. The use of two antibodies in this manner allows for the same secondary antibody to be utilized for the labelling of different molecules in different conditions by multiple primaries of the same species and greatly simplifies the production and use of primary antibodies by not having to conjugate a fluorescent marker. It should be noted however that this increase in ease of use also usually increases the amount of background fluorescence when imaging.

Our lab has previously utilized indirect immunofluorescence labelling to visualize ABCC5 in the GLUTag mouse cell line and mouse ileum (Fig 1.4). The labelling protocol developed for murine cells and tissue was unsuitable for the human NCI-H716 model L cell line we intended to use in future experiments (Fig 3.2). Optimization of the labelling protocol for human ABCC5 began with testing different antibody types available (Fig 3.3). However, a mouse monoclonal antibody (Fig 3.3A), a rabbit polyclonal antibody (Fig 3.3C), and a goat monoclonal antibody (3.3E) all produced a faint, diffuse signal within the stained cells. Poor labelling is often caused by inappropriate fixation of samples, for which most protocols use dissolved paraformaldehyde or neutral buffered formalin (NBF) as a fixative [48, 49]. However, changing the duration of fixation (5, 10, 15, 20, or 30 minutes) or the dilution of NBF (1%, 2.5%, 5%, or 10%) did not meaningfully improve labelling. The method of fixation itself can potentially contribute to a lack of signal, as NBF crosslinks proteins together and may reduce the antigenicity of target proteins. Indeed, fixation with 100% methanol significantly improved the signal intensity using the same antibodies previously tested (Fig 3.3 B/D/F).

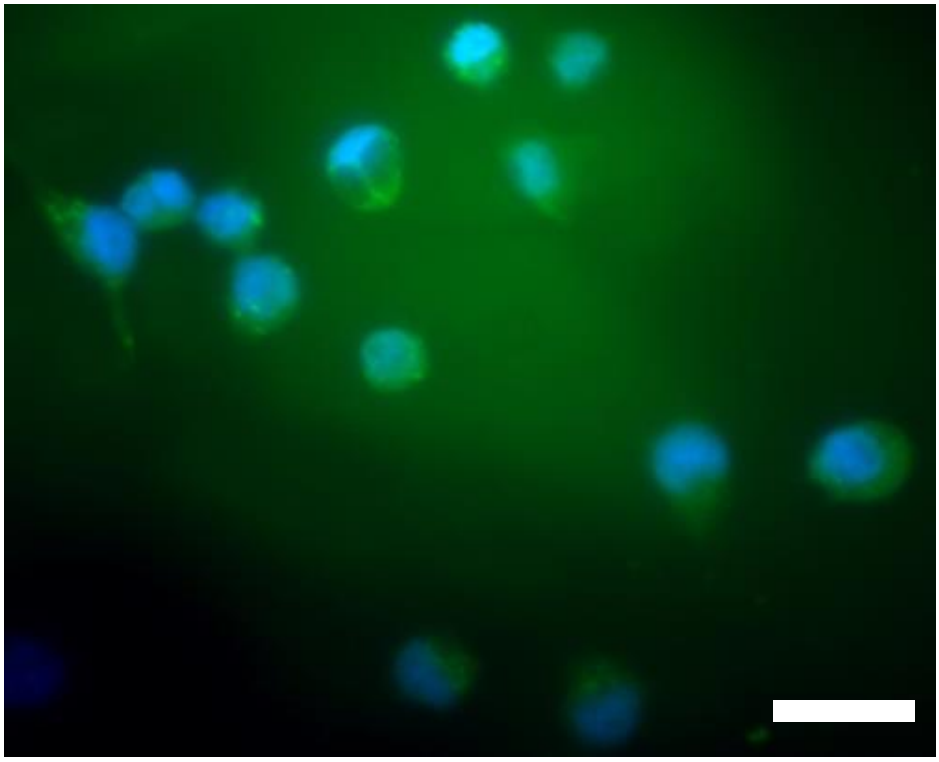


**Figure 3.2 –** Unoptimized immunofluorescence stain for ABCC5(green) in NCI-H716 cells. Cells were fixed using standard NBF protocol outline in methods. Scale Bar = 20µm

Due to the strong labelling and the availability of the mouse monoclonal antibody against ABCC5 [sc-376965], colocalization experiments were performed using this antibody. Further troubleshooting to optimize the incubation temperature and duration for the primary and secondary antibodies[50] yielded a suitable protocol for visualizing ABCC5, which reliably produced strong labelling with low apparent background (Fig 3.4). Each experiment also included a labelling control, a condition with no antibodies added to assess for autofluorescence, and secondary antibody controls, in which one or both primary antibodies are excluded to ensure there is minimal or no cross reactivity or nonspecific binding, respectively[29, 49, 51].

Due to difficulty in obtaining a strong signal, we decided to prioritize the fixation protocol for our protein of interest for these colocalization experiments. Another important aspect of these imaging experiments necessitated by the relative weak signal for ABCC5 is the use of a widefield microscopy instead of a confocal imaging system. Confocal microscopy is often the preferred method for colocalization analysis as the removal of out of focus light significantly improves image

clarity and z-axis resolution[52, 53]. During colocalization it is important to minimize the likelihood that a colocalized pixel erroneously occurs from two targets with similar x- and y-axis position but differ on the z-axis, particularly as our putative structures are smaller than the resolution of the microscope (~200-250nm). Additionally, out of focus light produced by fluorophores above and below the focus plane can skew attempts to quantify the degree of colocalization by introducing a high background of 'colocalized' scattered light. However, to occlude the majority of scattered light a confocal microscope discards about 90% of the signal[52, 54]. The photomultiplier tubes used in a confocal system are also significantly less sensitive than the cameras within a widefield microscope. Widefield microscopy was therefore chosen for its sufficient sensitivity to image the relatively weak signal within our stains[55, 56]. Images were also acquired as whole z-stacks of cells and processed with constrained iterative deconvolution software.

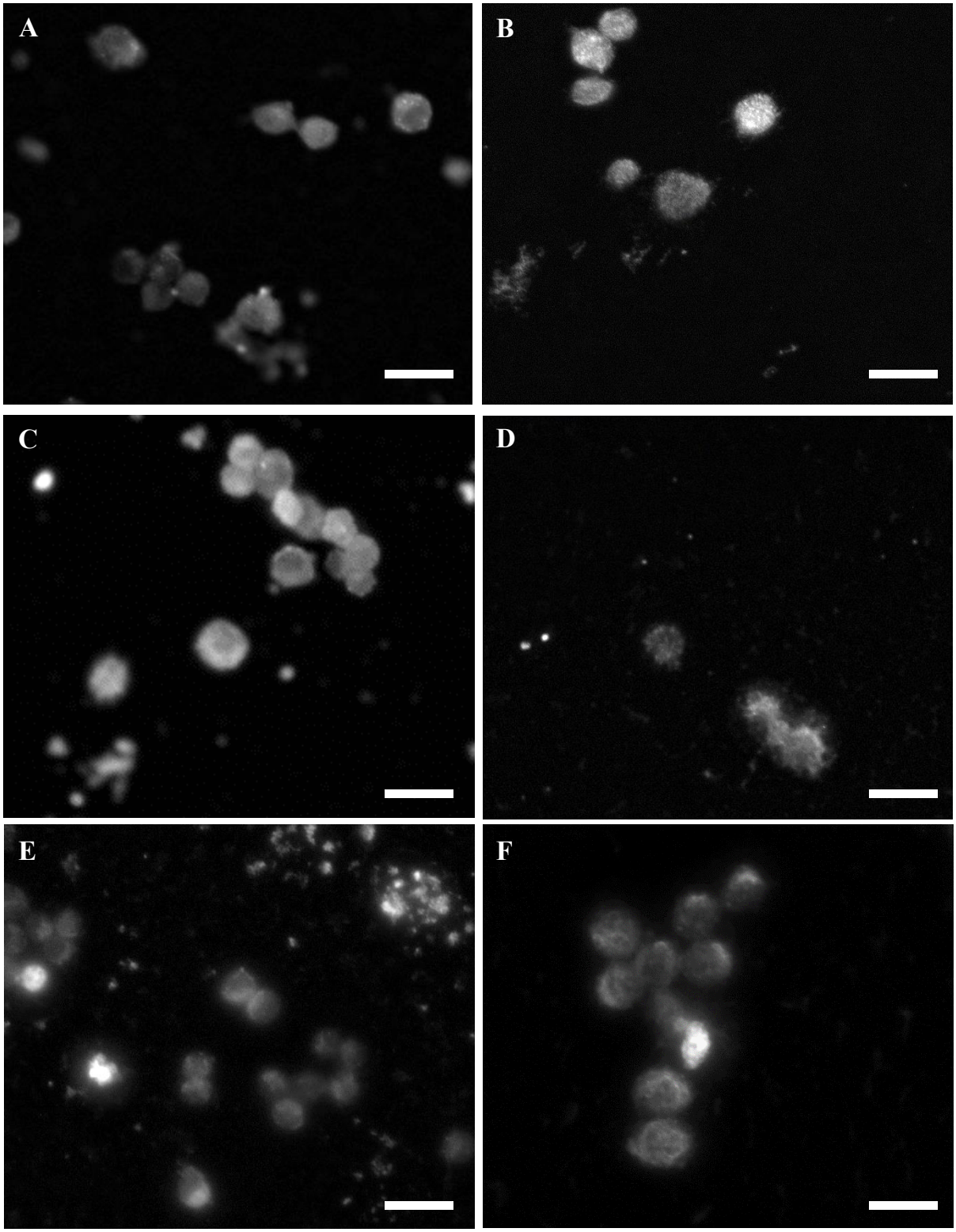



**Figure 3.3 –** Optimization of ABCC5 Immunofluorescence Stain. NCI-H716 cells were fixed with either NBF (A,C,E) or methanol (B,D,F). Cells were then immunostained with different antibodies targeting ABCC5, either (A,B) mouse monoclonal antibody [sc-376965], (C,D) rabbit polyclonal antibody[sc-20769], or (E,F) goat monoclonal antibody [sc-5781]; represented in greyscale. Scale bar = 20µm

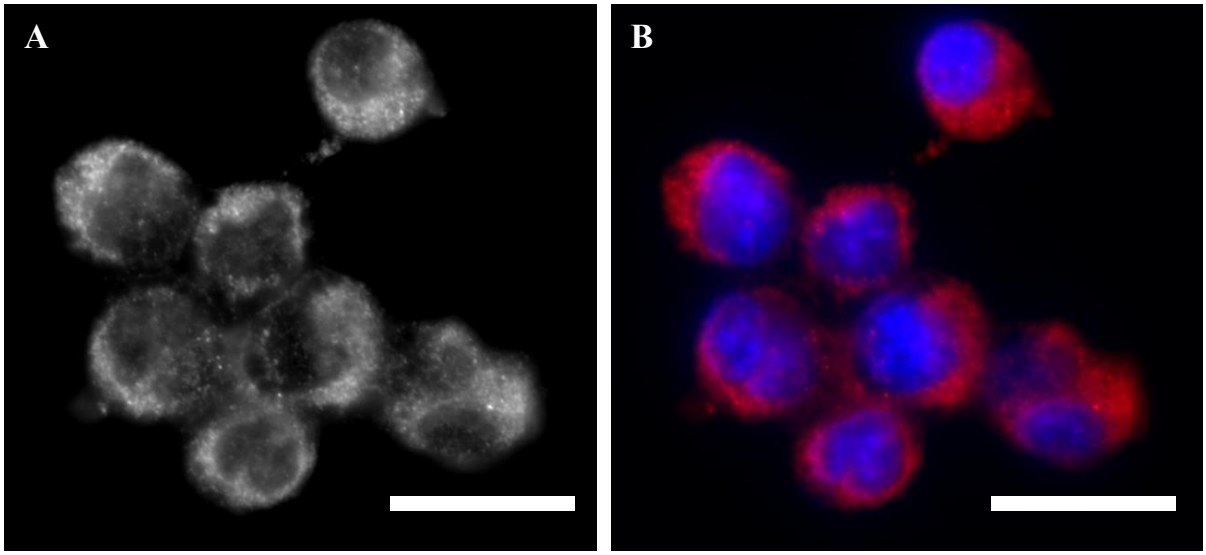



**Figure 3.4** Optimized ABCC5 immunolabelling Methanol fixed NCI-H716 cells were labelled with mouse monoclonal antibody [sc-376965] for ABCC5. Representative images showing (A) ABCC5 only and (B) ABCC5 (red) with nuclear counterstain. Nuclei stained with DAPI, shown in blue. Scale bar = 20μm.

## 3.3 **Results**

To determine the cellular localization of ABCC5, immunohistochemical analysis was performed on methanol-fixed NCI-H716 cells using a high-resolution widefield microscope (Fig 3.5). ABCC5 produced a punctate distribution of fluorescence and was not associated with the cell membrane. Dual labelling for ABCC5 and either GLP-1, VGLUT2, or LAMP2 showed that none of these markers colocalized with ABCC5. Unfortunately, due to the closure of core imaging facilities caused by COVID-19, colocalization of ABCC5 with synaptophysin was unable to be performed. The expression of ABCC5 was also investigated within primary gut cell cultures from murine intestines, where a strong punctate pattern of fluorescence was also observed (Fig 3.6 A/B). ABCC5+ cells represented only a small population of cells relative to the total number of cells within the slide and had morphology typical of enteroendocrine cells. Primary gut crypt preparations were also stained for GLP-1 to identify enteroendocrine cells (Fig 3.6 D/E), but additional dual labelling for ABCC5 and GLP-1 was hindered by time constraints and closure of animal facilities due to COVID-19.

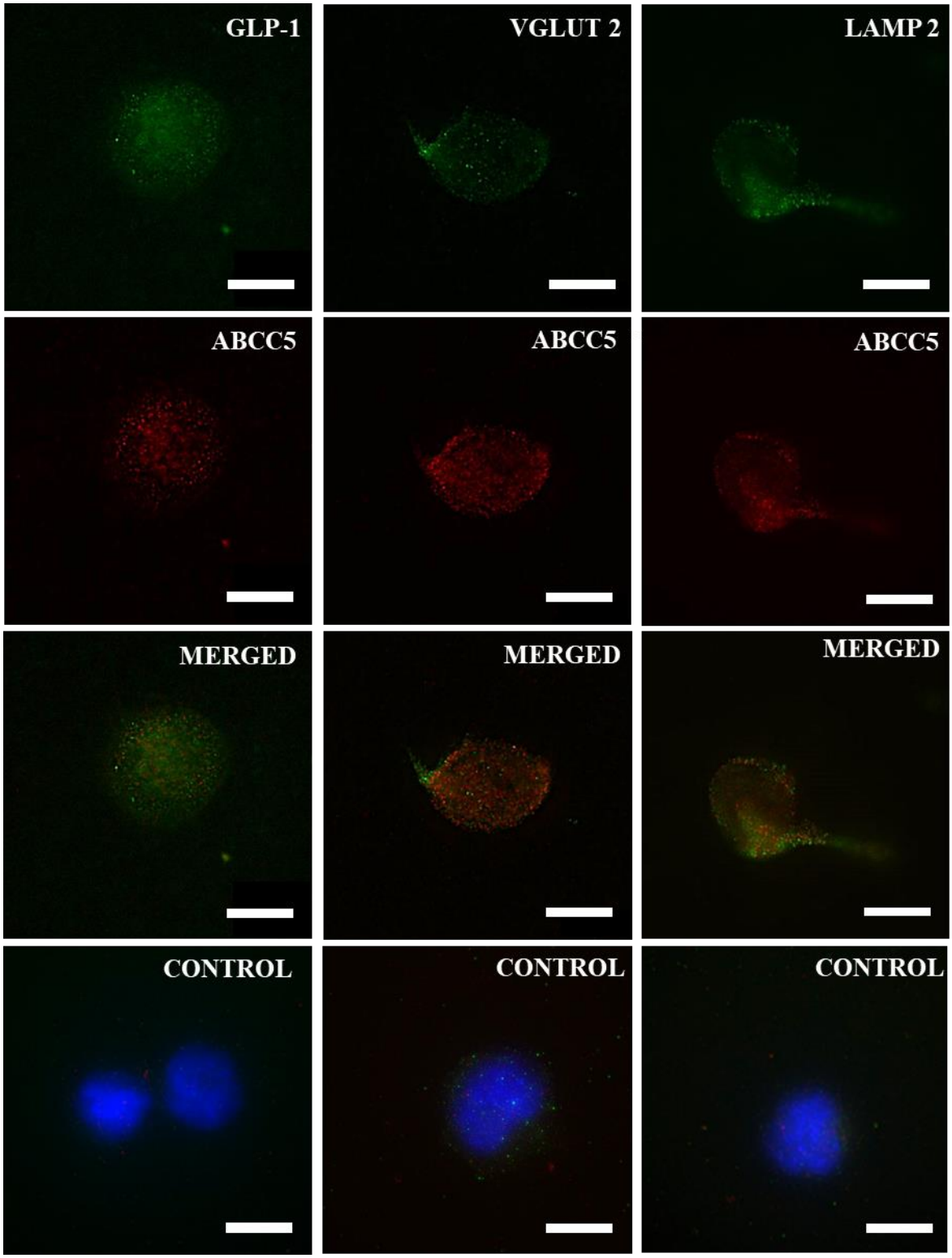



**Fig 3.5 –** Expression and localization of ABCC5 within NCI-H716 cells. Images show a single z-slice through the middle of the imaged cell. Cells were double immunostained with ABCC5 and anti-GLP-1 antibody(left), anti-VGLUT2 antibody (middle), or anti-LAMP2 antibody (right). Merged images also shown. No primary antibody control shown as max intensity z projection. At least 3 cells were imaged per condition. Acquired using Deltavision Elite inverted WF microscope, 100x 1.4NA objective. Scale bar = 10μm.

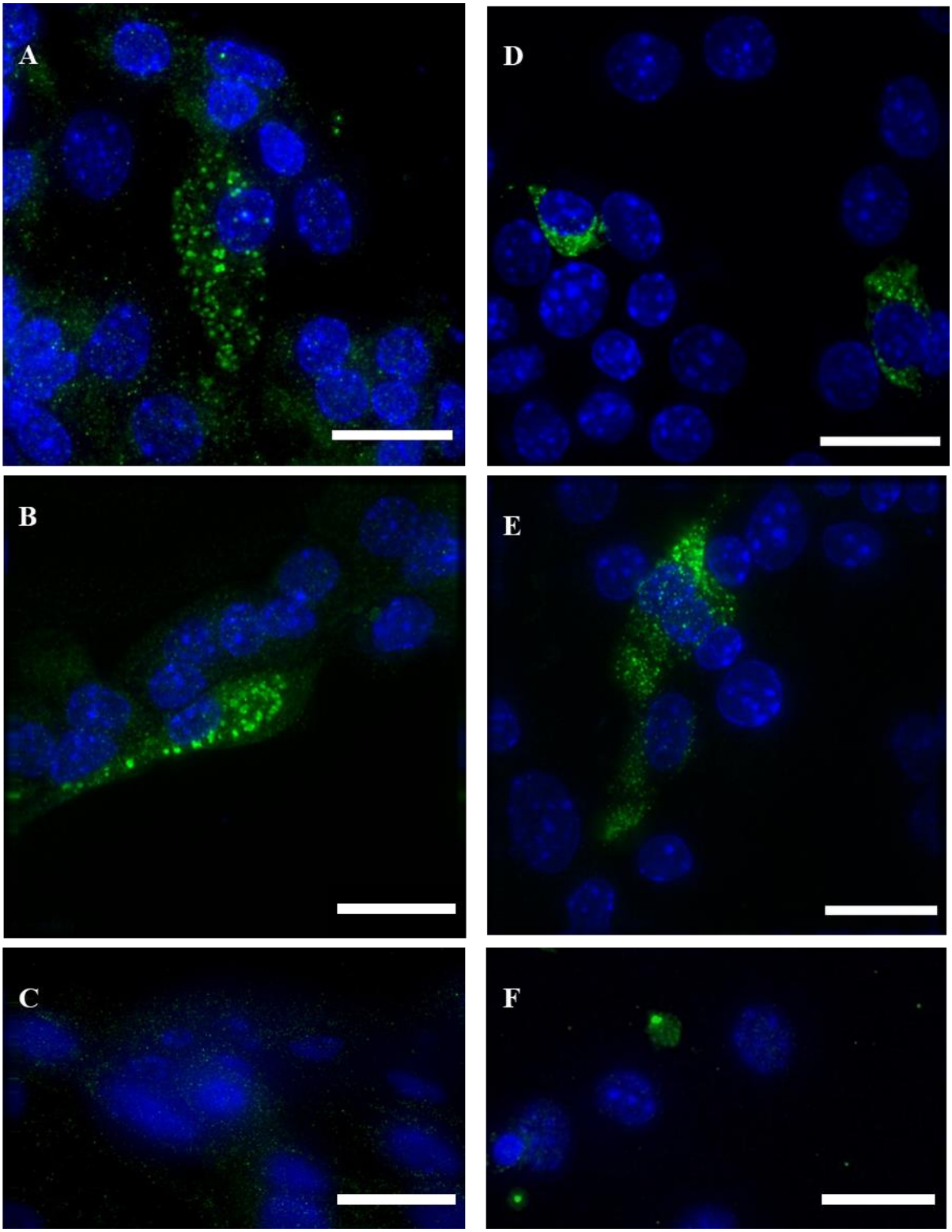



**Fig 3.6 –** Expression of ABCC5 and GLP-1 in primary gut crypts from mice. Representative z-projection images of ABCC5+ cells (**A, B**) and GLP-1+ cells (**D, E**). Primary gut cultures were immunostained for ABCC5 [sc-20769] or GLP-1, shown in green. Nuclei stained with DAPI, shown in blue. No primary antibody control(C, F) shown as max intensity z projection. Acquired using Deltavision Elite inverted WF microscope, 100x 1.4NA objective. Scale bar = 20µm.

## 3.4 **Discussion**

The results of these imaging experiments suggest that ABCC5 has an intracellular, punctate distribution of expression and is not present at the plasma membrane of enteroendocrine cells. This intracellular pattern of expression is contrary to the predominant localization of ABCC5 to the cell membrane[57-60], and has not been observed in other ABCC transporters. ABC transporters are usually associated with the cell membrane[61, 62], with the notable exceptions of ABCA2-3 shown to function in lysosomal sequestration[46] and several ABCB transporters that enable intracellular peptide trafficking[63]. Additionally, the lack of significant ABCC5 surface expression suggests that the intracellular signal is not the result of trafficking intermediates between the ER and the cell membrane.

Unfortunately, quantitative colocalization analysis of the dual labelled images was not possible due to excessive background signal introduced by image layers above and below the focus plane. The relatively low signal to noise ratio also likely contributed to the inability to run the colocalization software "Coloc2" in ImageJ. Analysis of the images was only possible after processing the images with high thresholding, which excessively manipulates the original images. Ultimately, the quality of the images was insufficient to conclude the colocalization of ABCC5 with any of the targets tested. A significant increase in the signal to noise ratio or the use of a confocal microscope, and preferably both, will likely be required before quantitative analysis can be performed. At present, there appears to be a lack of colocalization between ABCC5 and GLP-1, VGLUT2, and LAMP2; however, these observations are purely qualitative and subjective.

The labelling protocol used for colocalization between ABCC5 and hypothesis-specific or general cellular markers was predominantly optimized to maximize the signal for ABCC5. The use of methanol fixation is perhaps the most drastic departure from the manufacturer recommended protocols for the non-ABCC5 targeting antibodies used in our experiments. The signal from

individual stains for the non-ABCC5 antibodies using the ABCC5-optimized protocol was indeed significantly weaker than control stains performed using their individual manufacturer outlined protocols. Ultimately, the development of a model L cell line or a mouse line in which expressed ABCC5 is tagged with a transgenic fluorescent protein would provide a strong, highly specific labelling of ABCC5 that allows for relative freedom to optimize an immunocytochemistry protocol for colocalization with other markers of interest. Alternatively, assessment of anti-ABCC5 antibodies from other manufacturers could determine an antibody more suitable for multilabelling. The improvement of fluorescent signal intensity would also potentially enable the use of confocal microscopy or even super resolution techniques.

The immunolabelling of primary gut cells has provided a high-resolution visualization of ABCC5 in the mouse intestine. It should be noted that the cells expressing ABCC5 cannot be classified as L cells at this time, as coexpression with GLP-1 or other gut hormones was not confirmed. However, the cells containing ABCC5 were of similar morphology and frequency as GLP-1+ cells from the same mouse intestine preparation. A preliminary attempt to multistain for ABCC5 and GLP-1 yielded too weak of a signal for ABCC5 and will likely require troubleshooting to optimize labelling similar to that for the NCI-H716 cell line.

# 4 Results: Live Cell Fluorescence Imaging

## 4.1.1 Introduction: Fluorescein Diacetate

The conjugation of fluorophores to antibodies is undoubtably a valuable tool for specifically visualizing targets of interest. Soluble, unconjugated fluorophores can also allow for specific structures to be visualized when paired with careful chemical and experimental design. Fluorescein diacetate (FDA) is a modified form of the fluorophore fluorescein and formerly used as a cell viability dye [64, 65]. The addition of two acetaldehyde groups to fluorescein makes FDA a non-polar molecule able to passively diffuse across the cell membrane (Fig 4.1A). Intracellular esterases then hydrolyze FDA back into fluorescein (Fig 4.1B), which cannot readily leave the cell due to its polarity.

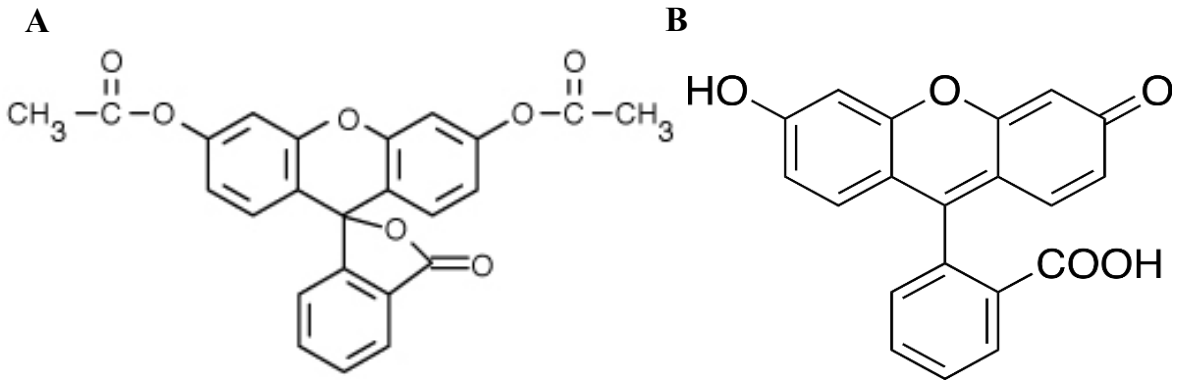



**Figure 4.1 –** Molecular structures of (A) fluorescein diacetate (FDA) and (B) fluorescein.

ABCC5 expression at the cell surface has previously been shown to reduce cell staining by FDA[35, 66]. Shipp *et al*[35] showed that overexpression of ABCC5 in sea urchin embryos caused significant reduction in the intracellular accumulation of FDA following a short incubation period. McAleer *et al*[66] expressed ABCC5 in HEK293 cells and also found FDA accumulation to be significantly reduced, and then used FDA accumulation to measure the effects of various drugs on ABCC5 transport activity. Additionally, both studies found that the reduction in labelling appeared to be specific to FDA as the effect was significantly less pronounced for other fluorescein-based dye variants and nonexistent with calcein, rhodamine, and BODIPY-based dyes. The inverse

relationship between ABCC5 expression and the amount of fluorophore within a cell strongly suggests that fluorescein is a substrate of ABCC5. Fluorescein is negatively charged at cellular pH[67], which is also consistent with the organic anion exporter function of ABCC transporters[68, 69].

Our current research hypothesis places ABCC5 as a vesicular transporter that maintains its outward-facing transport directionality, loading substrates from the cytoplasm into the vesicle lumen. We therefore would expect vesicular ABCC5 to transport FDA-derived fluorescein into vesicles and cause punctate fluorescent accumulation in addition to the general concentration of fluorescence seen within viable cells.

## 4.2 **Results**

NCI-H716 cells, a human model L cell line, were loaded with FDA for 5 minutes to allow for the fluorochrome to diffuse into the cells and be converted into active fluorescein. Cells were then thoroughly quickly washed for 90 seconds to remove extracellular FDA and imaged immediately or incubated for additional 10-minute intervals. Representative images of NCI-H716 cells at different incubation times following the initial FDA staining incubation are shown in Figure 4.2. Discrete clusters of increased fluorescence within cells are visible at all time points. The intensity of the background fluorescence also steadily increases overtime as fluorescein leaks from the cells, reducing the apparent contrast between the intracellular and extracellular compartments. After 20 minutes of additional incubation a punctate signal is still observed in approximately half of the cells, and after 30 minutes punctate accumulation is present in only a fifth of cells.

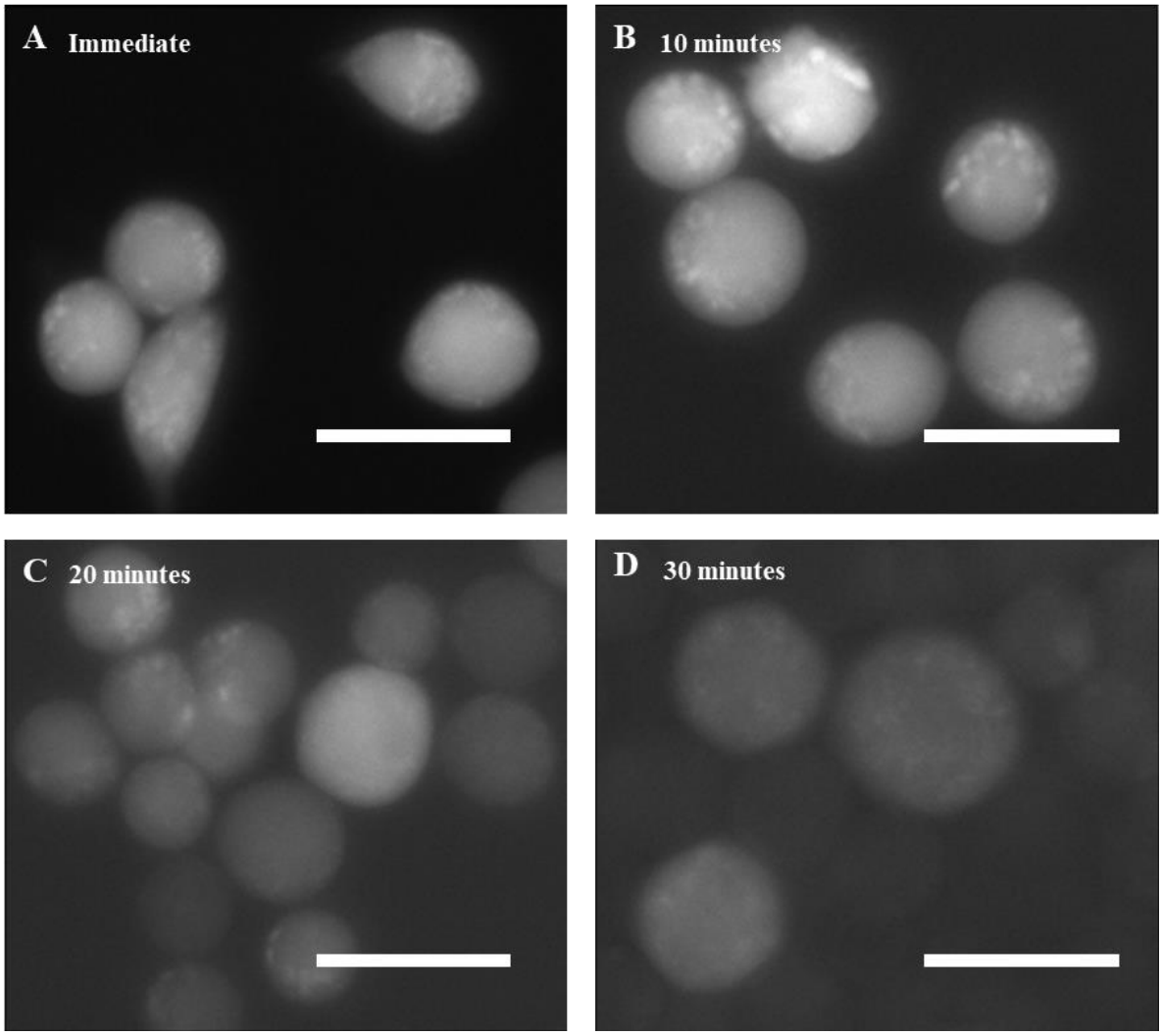



**Figure 4.2 – Live cell staining of NCI-H716 with FDA** (A-D) Representative micrographs showing the accumulation of FDA-derived fluorescein within human NCI-H716 cells. Representative of 2 replicate experiments, at least 3 images were acquired per condition. Incubation time elapsed after FDA loading before imaging: (A) immediate, (B) 10 minutes, (C) 20 minutes, (D) 30 minutes. Acquired using EVOS AMF4300 microscope with 40x 0.65NA objective. Scale Bar = 20 µm

## 4.3 Discussion

The results of these experiments suggest the feasibility of a technique to visualize the vesicular activity of ABCC5 within live model L cell lines using the common viability dye FDA. This protocol could allow for future investigation into the behaviour of ABCC5+ vesicles during enteroendocrine cell stimulation and potentially their exocytosis. Taken together, the fixed cell and live cell imaging experiments suggest that ABCC5 may be within vesicles and have transport activity.

A key experiment necessary to be confident that the observed punctate signal is attributable to ABCC5 is a negative control for ABCC5. This FDA treatment has also been tested in *ex vivo* gut crypts from ABCC5 KO mice and no punctate signal was observed. However, due to the rarity of enteroendocrine cells in these preparations (~1:1000) it is insufficient as a negative control. A repeat of this experiment in an ABCC5 knockout NCI-H716 cell line is required before the FDA accumulation can be stated to be ABCC5 specific. The transport of fluorescein may also competitively inhibit the transport of endogenous substrates by ABCC5 and thereby alter normal vesicle or cell behaviour. An important yet relative simple additional experiment that should be performed before utilizing this protocol further would be to include known ABCC5 inhibitors such as MK-571 or sildenafil[70, 71] as negative controls. Although these inhibitors also effect transport by other ABCC transporters, this experiment would increase our confidence that the observed puncta are attributable to ABCC5.

Another point of concern within this assay is the pH sensitivity of fluorescein, whose emission intensity is directly proportional to the ambient pH value[67]. Our observed discrete increases in fluorescence intensity may therefore be partially attributable to variations in pH between the cytoplasm and organelles. However, this scenario is unlikely as mitochondria are the only common organelles with pH significantly higher than the cytoplasm[72] and the observed areas of increased fluorescence do not have mitochondrial morphology. Nonetheless, if we intend to utilize this protocol more rigorously in the future, Mito Red [Sigma-Aldrich, 53271] is a rhodamine-based dye that could be loaded into cells alongside FDA and address whether the increased fluorescence intensity colocalizes with mitochondria. Conversely, the pH of secretory vesicles is significantly lower than the cytoplasm due to the prevalence of active $H^+$ pumps and highly controlled $H^+$ efflux[73]. The emission intensity of fluorescein within secretory vesicles would therefore be significantly reduced. For the fluorescent signal within secretory vesicles to be greater than the

cytoplasm, the fluorescein concentration within the vesicles would have to be significantly higher compared to the cytoplasm, which further suggests active loading by a transport protein.

Repeating this assay using a high-resolution fluorescence microscope equipped with a temperature- and atmosphere-controlled chamber would allow for continuous image acquisition and measurement overtime of fluorescence intensity individual cells and puncta. Additionally, the images shown here were acquired using a low-resolution microscope with minimal optimisation settings, which significantly limited the contrast within the images and our ability to discern structures of interest and their features.

Importantly, the high degree of fluorescein retention within the NCI-H716 cells for at least 10 minutes greatly increases our confidence that ABCC5 is not expressed or functional at the cell membrane of our model L cell line. Similar FDA staining in *Sp*-ABCC5a+ sea urchin pigment cells showed a near complete lack of intracellular fluorescein after 10 minutes of additional incubation following FDA loading[35]. The putative ABCC5 bearing vesicles are also therefore unlikely to be intermediates in the trafficking of the transporter towards the cell membrane; this is in agreement with the prior fixed cell immunofluorescence labelling that suggests ABCC5 is not at the cell surface (Fig 3.4/3.5). Moreover, the lack of fluorescein clearance from the cells suggests that other ABCC transporters, which are also organic anion transporters and able to transport fluorescein[74], are not expressed at the cell membrane in this model. However, this a theoretical assumption and must be confirmed using an ABCC5 knockout NCI-H716 cell line.

These results suggest that FDA could be used to track the activity of ABCC5 in model L cell cultures using live cell imaging. This method could allow for investigation into the behaviour of ABCC5+ vesicles during cell stimulation. Understanding the mobility of ABCC5-bearing vesicles can provide evidence for whether these vesicles are concurrently released with GLP-1 secretory granules or are governed by different mechanisms.

# 5 Results: NAAG-$^{13}C_5$ Vesicular Transport Assay

## 5.1.1 Introduction: Membrane transporters and Vesicular transport assays

Membrane transport proteins are essential for mediating the exchange of materials across the cell membrane and internal membranes. Functional characterization of transport proteins can now be performed through a diverse array of techniques depending on the nature of the transporter and substrate of interest. The principal components for a transport assay include the production of liposomes containing the transport protein in question, initiation of transport with the introduction of energy and the desired substrate(s), and the termination of uptake and detection of changes in substrate distribution between external and internal compartments[75].

Several methods have been developed to produce lipid bound compartments with which transport activity can be assayed. Intact cells are a commonly used model in uptake assays due to the relative ease of altering the cell membrane expression of the transporter of interest and the minimal preparation required to conduct the assay itself[75]. However, the metabolic pathways active in live cells can often alter transported substrates and prevent accurate quantitative measurement. Right side out membrane vesicles (RSOVs) and inside out membrane vesicles (IOVs) can also be generated from the outer membranes of cells or other expression systems, which eliminate disruption by the cell metabolism but still include all of the other integral membrane proteins expressed in the system. Purified transport proteins can be reconstituted within liposomes to generate artificial proteoliposomes that provide a controlled model in which the activity of a specific transporter can be isolated. These techniques allow for novel substrates for transporters to be investigated and the quantification of transport dynamics.

Both cell surface overexpression and artificial liposomes have previously been used to demonstrate that ABCC5 is capable of transporting NAAG and other glutamate conjugates[3]. However, neither of these techniques replicate the $H^+$ electrochemical gradient generated by the vacuolar $H^+$-ATPase

pump, which is a major characteristic of vesicles and essential for classical vesicular neurotransmitter loading[76]. Indeed, the vesicular loading of NAAG has been previously shown to be catalysed by a member of the solute carrier family, SLC17A5, which is a large group of secondary active transporters whose transport is coupled to the electrochemical gradient. In order to determine whether ABCC5 directly participates in the vesicular loading of NAAG, the transport assay utilized must incorporate all of the physiological components of endogenous vesicles. This not only includes the vacuolar $H^+$-ATPase but also the many other transporters and integral proteins likely present within ABCC5-bearing vesicles. The use of a physiological model for our uptake assay would allow us to clarify whether the known NAAG-transport capacity of ABCC5 is relevant within endogenous SLMVs or alternatively that ABCC5 likely influences NAAG transport or metabolism through indirect mechanisms. We therefore decided to utilize purified *ex vivo* murine SLMVs as a direct source of membrane-associated transport protein for our transport assay.

### 5.1.2 **Nuclear magnetic resonance spectroscopy**

Transported substrates are conventionally labelled for detection following the transport assay using radioisotopes within the molecule[75]. Isotopic labelling provides a robust signal measurable with relative ease in a scintillation counter, and outweighs the additional safety measures the technique warrants. When radiolabelling is unsuitable, transport may also be indexed through a fluorophore bound to the substrate itself or the addition of a fluorescent indicator responsive to changes caused by the transport process[77]. However, neither of these labelling methods was available or suitable and so we have utilized $^{13}C$-isotopically labelled NAAG for detection using nuclear magnetic resonance (NMR) spectroscopy.

NMR spectroscopy is an invaluable tool for investigating a range of chemical properties[78-80], and is now commonly used to investigate brain metabolism[81]. To briefly summarize, atomic nuclei that are NMR active, for example $^{1}H$, $^{13}C$, and $^{31}P$, have an odd ratio of neutrons and protons, which

causes these nuclei to have an electrical charge and a nuclear spin. Application of a magnetic field to a sample causes the magnetic moments of the nuclei to align with that of the external magnetic field. Pulses of radiowaves drive the aligned nuclei into a higher energy state in which their magnetic moments oppose that of the external magnetic field. As the nuclei relax from the higher energy state back to the lower energy state, energy is emitted at the same frequency and can be measured. Repeated cycles of pulsing and relaxation are performed until the signal can be distinguished from background noise, and Fourier transformation of the recorded output frequencies produces a spectrum with peaks corresponding to the active nuclei. Spectra are then interpreted based on prior observations of how the chemical and magnetic environments of nuclei affect the relative shift and appearance of their peaks along the spectrum.

For our current applications we will utilize carbon-13 NMR to detect labelled nuclei within NAAG to determine its relative concentrations within different conditions from our vesicular transport assay. The NAAG-$^{13}C_5$ we are using is characterized by five $^{13}C$ nuclei that constitute the carbon structure of glutamate within NAAG (Fig 5.3A). Each $^{13}C$ nucleus produces a distinct peak along the NMR spectrum (Fig 5.3B). The first and second peaks from the left correspond to the two carboxylic acid groups and the third, fourth and fifth peaks are caused by the α, γ, and β carbons within the glutamate of NAAG (Fig 5.3B). The apparent differences in peak heights between the $^{13}C$ nuclei reflect differences in peak multiplicity (splitting) from interactions with neighboring carbon centers. Peak integration is the preferred value for measuring relative concentration when peak multiplicity is a factor and therefore will be the measurement used in our analysis[82, 83].

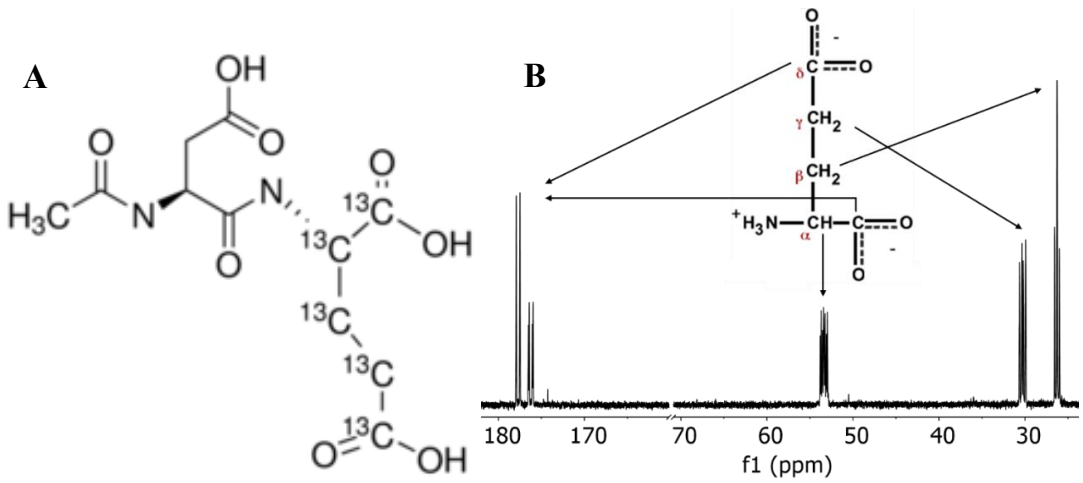



**Figure 5.1 –** Molecular structure of NAAG-$^{13}C_5$ (A) and its associated $^{13}C$ NMR spectrum (B) showing the mapping of $^{13}C$ peaks within the NMR spectrum of NAAG-$^{13}C_5$. Molecular structure is the labelled glutamate moiety of NAAG-$^{13}C_5$. ppm= parts per million.

## 5.2 **Transport Assay Development**

Our lab has adapted a protocol for the isolation of synaptic vesicles from mouse brains developed by Ahmed *et al*[38], in order to obtain suitable ABCC5 bearing vesicles with physiological relevance. This protocol ultimately consists of four differential centrifugations to separate vesicles from large membranes and cellular debris, followed by a sucrose gradient rate-zonal centrifugation to isolate vesicles from ribosomes and soluble proteins (Fig 5.2). Mouse brains were utilized as the source tissue instead of mouse intestine due to the low frequency of L cells within the intestines (~0.1%)[84]. This method also allows us to utilize our existing *Abcc5* KO mouse line as a negative condition in our transport assays. The yield and purity of vesicles within the fractions isolated from our adapted protocol was assessed by probing for synaptophysin[45] using a western blot and Coomassie stain. All fractions contained synaptophysin but fractions 10 through 19 were significantly enriched with the protein (Fig 5.3A). Conversely, the Coomassie stain of the same gel shows that the total protein content sharply declines between fraction 10 and fraction 11, with subsequent fractions showing minimal total protein content (Fig 5.3C). The observed maintenance of fraction synaptophysin content while total protein content is significantly diminished demonstrates the efficacy of the adapted vesicle isolation protocol.

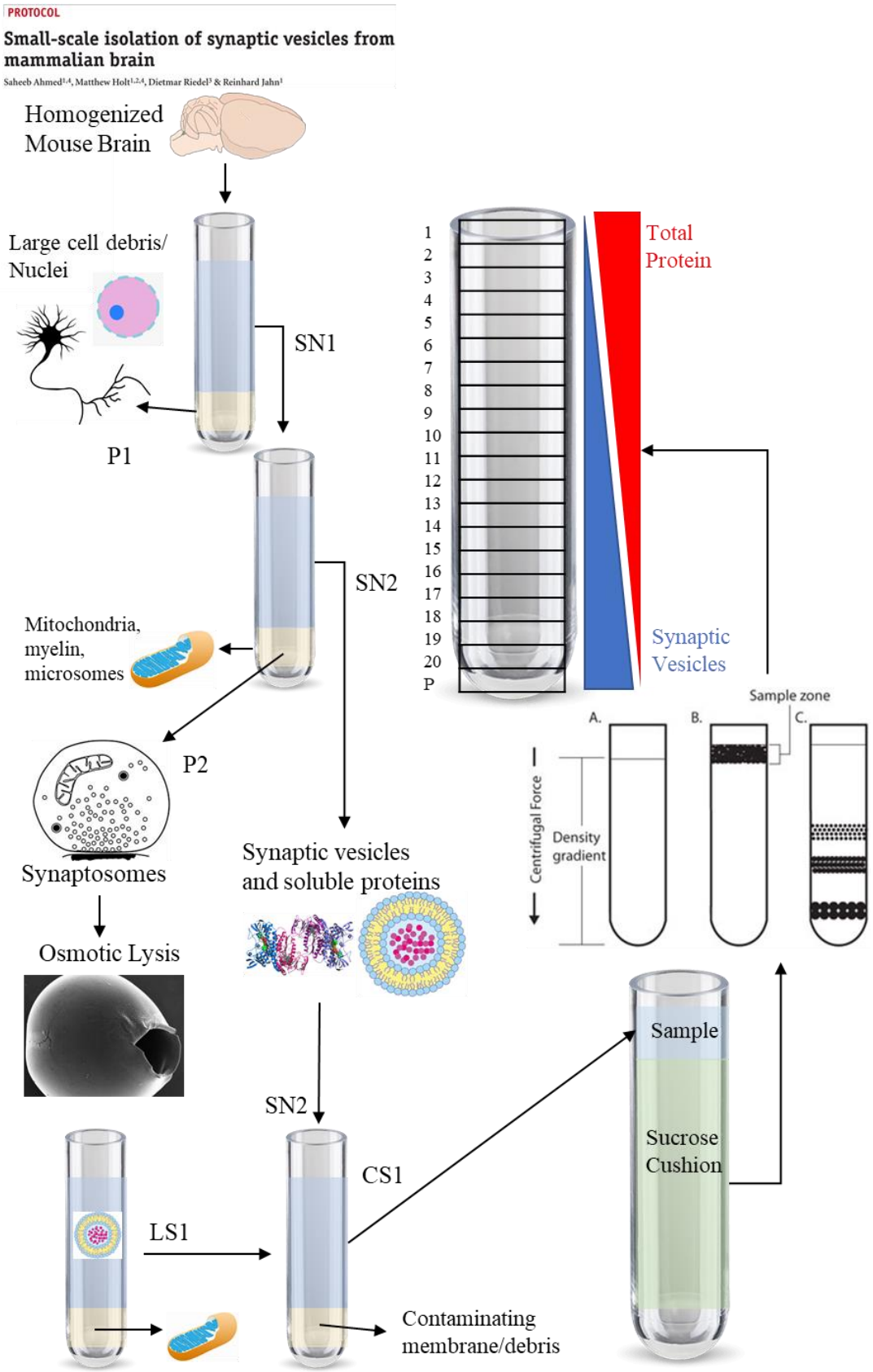



**Figure 5.2 –** Summary diagram of vesicle purification protocol, based on Ahmed *et al*[38]. Outlined in Section 2.4.2 in Materials and Methods

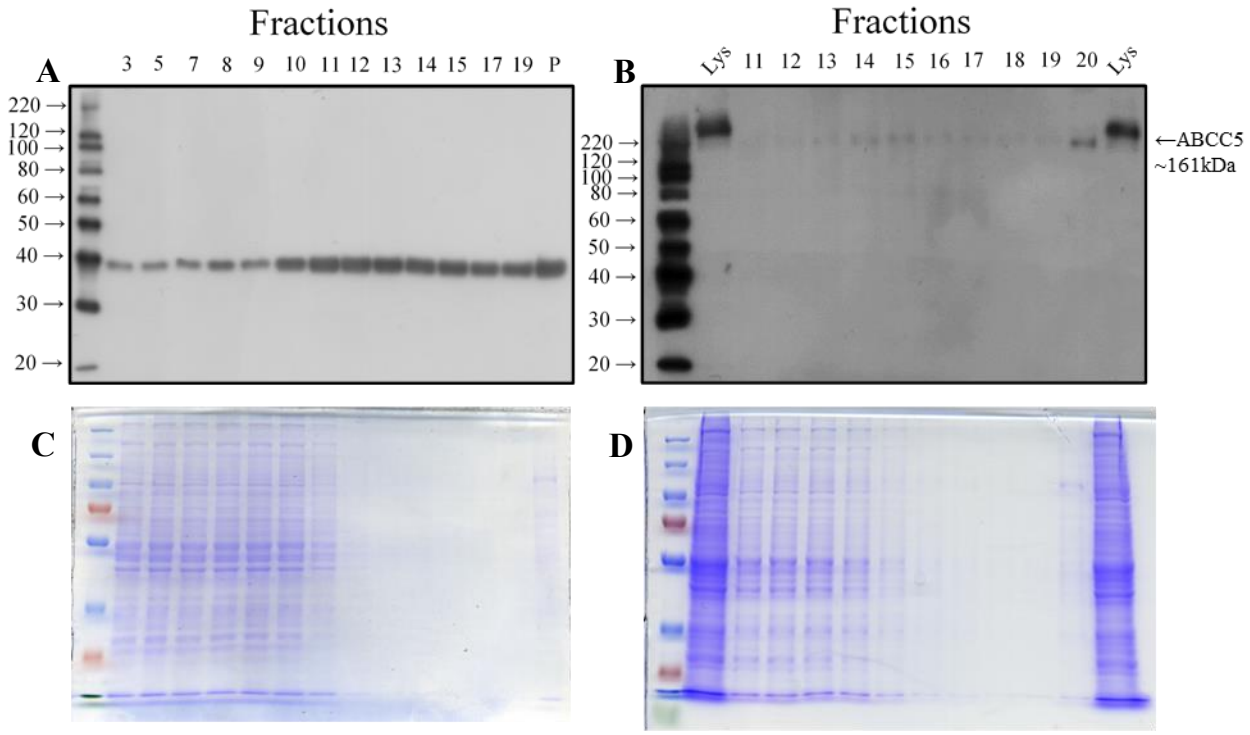



**Figure 5.3 –** Western blots of isolated fractions from vesicle purification preparation and associated Coomassie stains. (A)Western blot for synaptophysin and (C) Coomassie stain of gel. (B) Western blot for ABCC5 and (D) Coomassie stain of gel. MW synaptophysin 38kDa; ABCC5 161kDa.

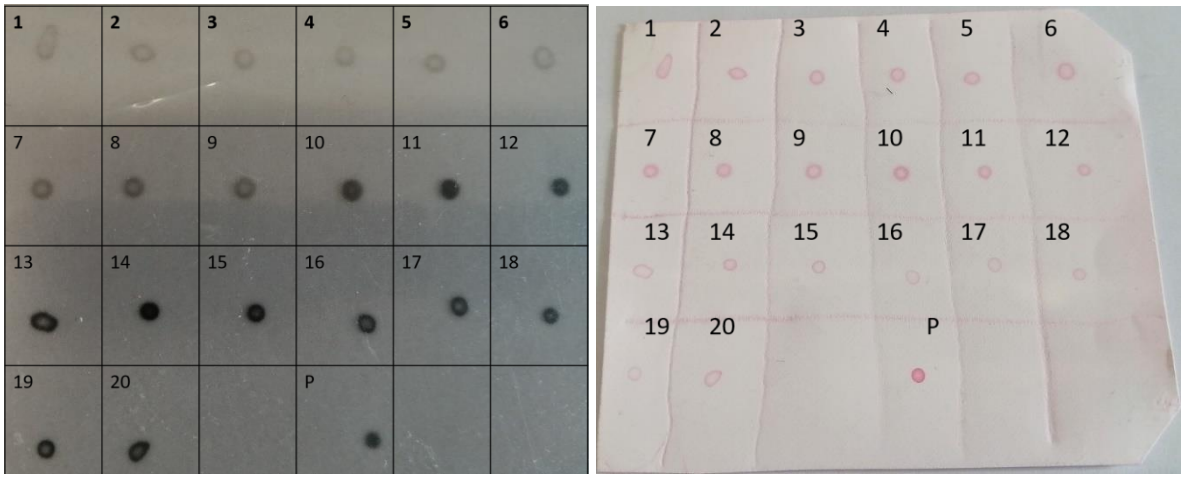



**Figure 5.4 -** Representative dot-immunobinding assay probing synaptophysin within fractions isolated from vesicle purification preparation as a quick fraction purity check, and associated Ponceau stain of the nitrocellulose membrane. P = pellet.

A dot immuno-binding assay probing for synaptophysin followed by a Ponceau stain of the nitrocellulose membrane was performed for each preparation to ensure consistent sample purity was maintained between samples and to quickly identify the fractions with sufficient purity (Fig 5.4). A western blot was also performed to probe for the presence of ABCC5 within the purified

fractions (Fig 5.3B). WT mouse whole brain lysate was used as a positive control for a known ABCC5-containing sample. Isolated fractions were shown to contain ABCC5, although in low abundance. However, it is important to note that the sharp decline in total protein content occurred between different fractions depending on the individual fraction preparation (Fig 5.3C-D).

Interestingly, two bands are visible from the whole mouse brain lysate samples when compared to fraction samples when probing for ABCC5 (Fig 5.3B). This dual banding seen in western blots staining for ABCC5 has been consistently observed by our lab and has been validated to not be the result of nonspecific binding or cross reactivity[29]. The presence of only one observable band within a sample purified to only contain ribosomes, soluble proteins, and small endosomes herein strongly suggests the existence of at least two isoforms of ABCC5: a vesicular, lower molecular weight variant and a higher molecular weight variant possibly expressed at the cell membrane or large organelles in the brain. The role of ABCC5 at the cell membrane is well established, particularly in the brain[57-60]. Alternative ABCC5 splice variants have also been previously described[85] as well as numerous post translational modifications[86, 87]. Repeating this western blot after deglycosylating the proteins within the whole brain lysate would answer whether this glycosylation is responsible for the disparity in molecular weight. Additionally, testing of the cell membrane containing P1 pellet from the vesicle purification process alongside the vesicles and lysate could confirm whether the higher molecular weight ABCC5 is located within the cell membrane. Similarly, this would increase our confidence that the lower molecular. In the future it would be worthwhile to investigate possible differences in behaviour between these ABCC5 variants as well as determine the cause(s) of their structural variation.

The results of our assessments regarding the efficacy of the vesicle purification protocol have replicated the controls performed by the original authors[38]. However, two additional control experiments could be performed to further assess the purity and viability of the vesicle purification. Negative staining electron microscopy could be performed on the purified vesicles to demonstrate

that the samples are not contaminated with membrane fragments or cytoplasmic debris[88, 89]. The morphology and size of purified vesicles can also be tested. In addition to retaining the composition and appearance of endogenous vesicles, the ability of vesicles to transport and store neurotransmitters should be assessed to ensure their *in vivo* functions are maintained following purification. A transport assay for $[^3H]_L$-glutamate is a recommended control experiment due to the relative abundance of $VGLUT^+$ vesicles and the dependence of glutamate transport on the electrochemical gradient. Failure to transport glutamate would suggest a disruption of membrane integrity or the loss of the vacuolar $H^+$-ATPase, which is a common problem of vesicle purification preparations[90]. We had been unable to perform this viability assay due to delays in obtaining the necessary license for radioactive substrates, but this experiment will be performed as soon as possible.

## 5.3 **NMR Results**

The protocol for this transport assay was adapted from the $[^3H]_L$-glutamate uptake assay recommended by the authors of the vesicle isolation method[38], who utilized an assay originally outlined by Hell *et al*[39]. A summary of the transport assay is outlined in Figure 5.6. Vesicles from both WT and KO will be assayed to determine whether the transport of NAAG is attributable to ABCC5 and to what degree, if any transport is observed. Additionally, each condition was performed with ATP ($^{+ATP}$) and without ATP ($^{-ATP}$) as a negative control. Finally, control conditions were included that contained no vesicles but were otherwise identical and processed in parallel to the WT and KO conditions.

The "assay buffer filtrate" in our experiment refers to the transport assay buffer that has passed through the membrane filter and been separated from the vesicles. The "vesicle eluate" is the vesicles and residual assay buffer after filtration that have been placed into an 80% methanol solution to release the vesicle contents. The separation of vesicles from the transport assay buffer

allows for distinction between transported NAAG (vesicle eluate) and untransported NAAG (assay buffer filtrate) by their confinement to the extra- or intra-vesicular compartments.

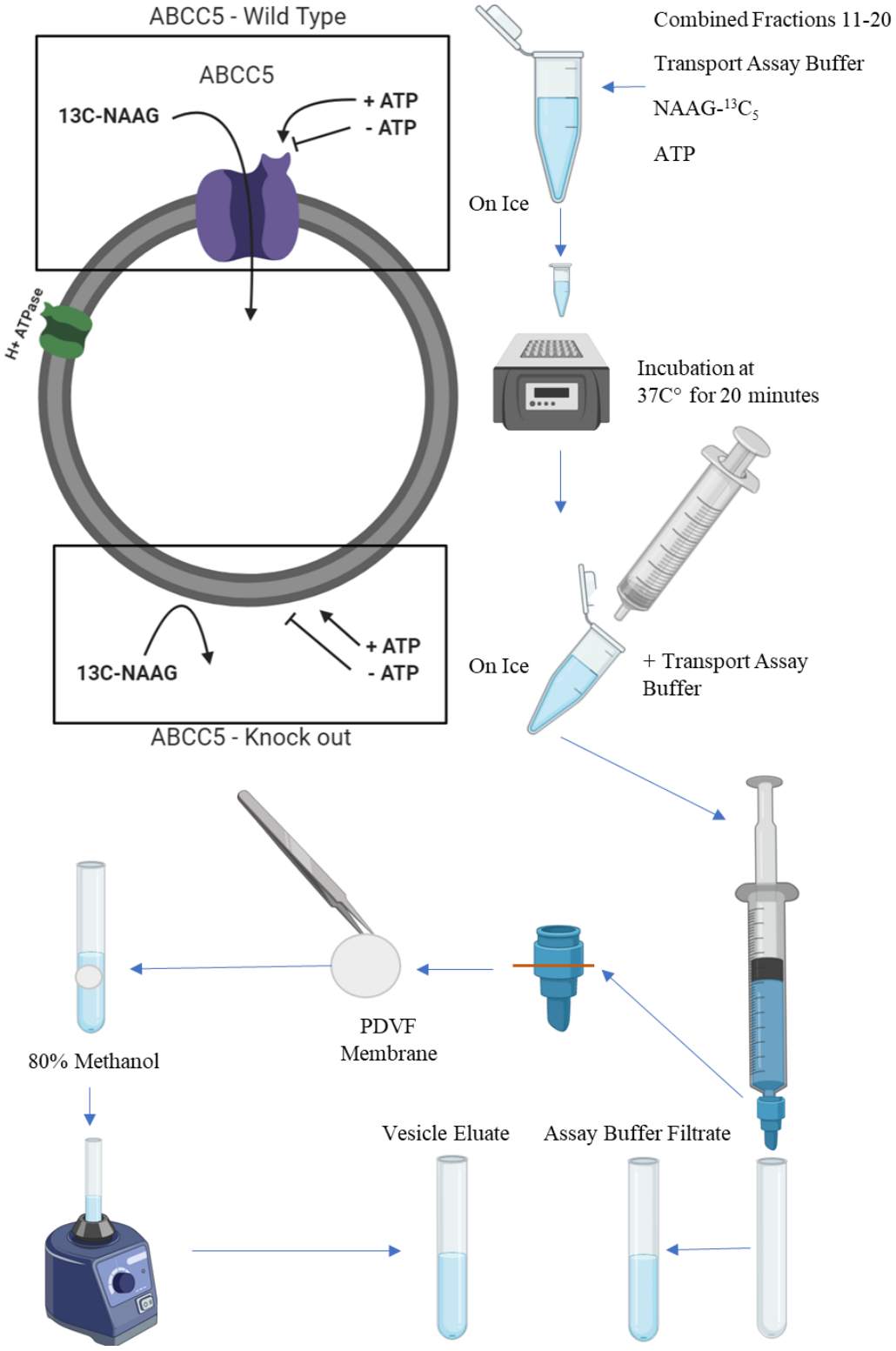



**Figure 5.5 -** Summary diagram of adapted vesicle transport assay. Outlined in Sections 2.5.2 and 2.5.3 in Materials and Methods

It should be noted that although the initial stages of the transport assay were performed as expected, a major difficulty was encountered during filtration. For all KO and WT sample conditions there was a sharp decline in flow rate soon after applying pressure and beginning sample filtration. As a result, filtration of the WT samples lasted for approximately 7 hours and for the KO samples approximately 8 hours, compared to 10 minutes of filtration time for the control (no vesicle) samples. This was likely caused by the proteins and lipid of the vesicles saturating the pores of the filter membrane and severely reducing its permeability. Once the samples were completely filtered, the remaining preparation of the vesicle eluates proceeded normally. Additionally, following all stages of the transport assay and separation of the assay buffer filtrate and vesicle eluate, a constant amount of maleic acid was added to each sample to serve as an internal reference control during analysis.

The relative signal intensities of NAAG in each sample are shown in Figure 5.6 A-B, with the original spectra summarized in Figure 5.6 C and a full example spectrum shown in Figure 5.6 D. The integral values of four NAAG-$^{13}C_5$-associated peaks from each condition were averaged to minimize the effect of detection noise. Samples were normalized using the peak intensity for maleic acid to account for variations in sample volume; this variation also meant it was impossible to meaningfully quantify absolute concentrations of NAAG by NMR in the final samples. The results of this preliminary vesicle transport assay are unfortunately inconclusive regarding the participation of ABCC5 in NAAG transport.

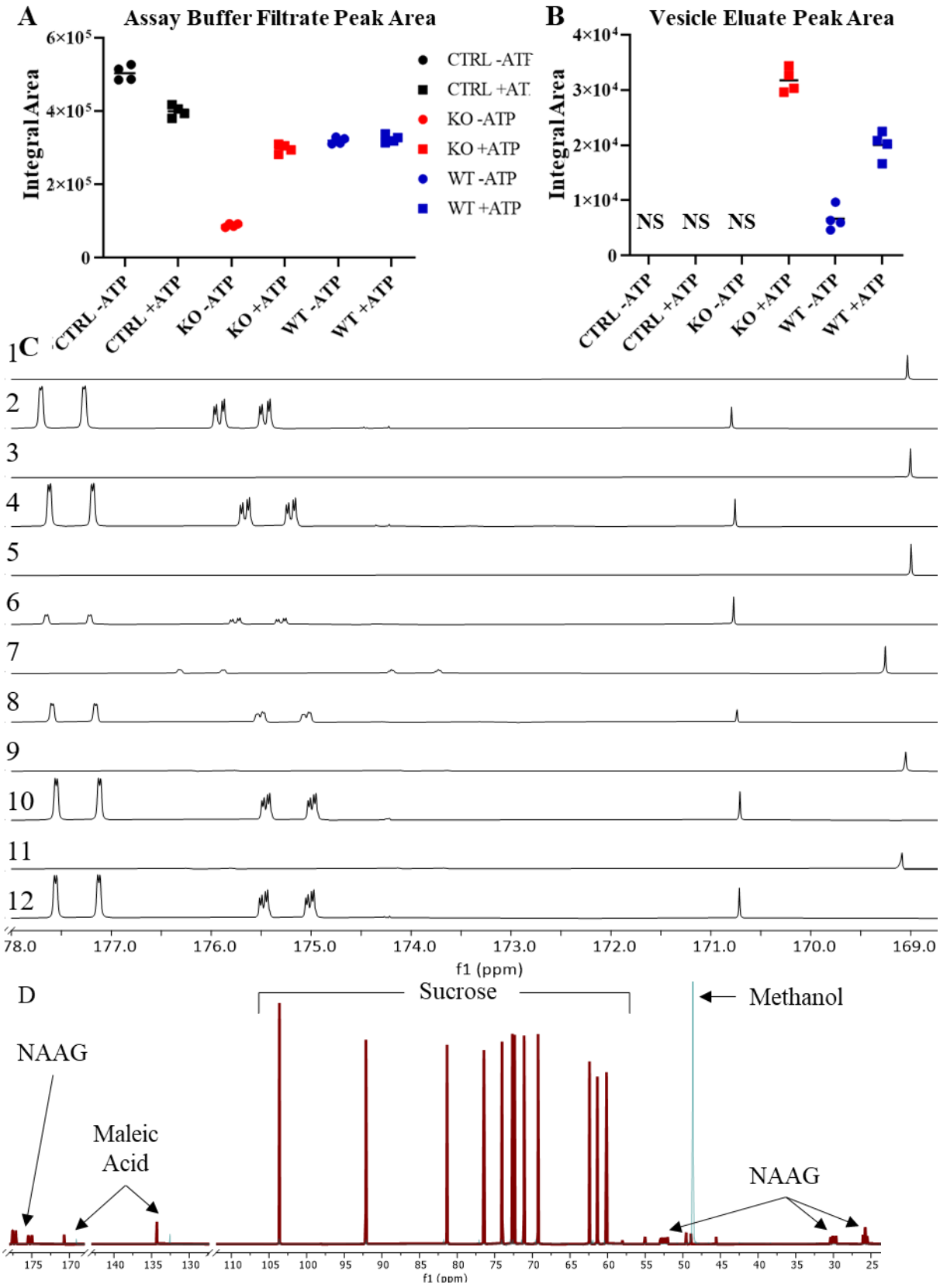



**Figure 5.6 -** Relative NAAG concentrations in vesicle transport assay and related spectra. NAAG-$^{13}C_5$ signal intensities were measured for each sample of (**A**) assay buffer filtrate and (**B**) vesicle eluate.

NS = no NAAG signal detected. Four points of each sample represent the four peak areas measured per condition and together represent one experiment. Y-axis values shown in arbitrary units. Results are presented as mean ± SD (n=1). (**C**) Stacked NMR spectra from preliminary vesicular transport assay. Vesicle eluate & Assay buffer filtrate conditions (ELU, FLTR): (1,2) CTRL -ATP, (3,4) CTRL +ATP, (5,6) KO -ATP, (7,8) KO +ATP, (9,10) WT -ATP, (11,12) WT +ATP. The rightmost peak corresponds to maleic acid. (**D**) Full unabridged spectrum of the WT +ATP assay buffer filtrate(red) and vesicle eluate(blue) samples.

## 5.4 **Discussion**

The results from this preliminary experiment greatly increase our confidence in the feasibility of a vesicular transport assay that utilizes NMR for substrate detection. This chapter has demonstrated the isolation of *ex vivo* synaptic vesicles from mouse brains and outlined a potential novel transport assay based on NMR-active substrate measurement. With procedural adjustments to prevent prolonged filtering times, this assay shows promise to be able to investigate the role of ABCC5 in the vesicular transport of NAAG and other substrates of interest.

When seeking to interpret the data from this transport assay, both the assay buffer filtrate and the vesicle eluate are useful for assessing whether transport has occurred. A loss of labelled substrate from the assay buffer filtrate and the gain of labelled substrate in the vesicle eluate would indicate that the substrate was transported from the transport assay buffer across the vesicle membrane. The lack of detectable NAAG signal within the vesicle eluates of our control conditions demonstrates both the efficacy of filtration and the necessity of vesicles within the transport assay solution to measure NAAG in the vesicle eluate. However, the assay buffer filtrate of the $WT^{-ATP}$ and $KO^{-ATP}$ conditions is not equivalent to the controls, which suggests that some NAAG may be retained on the surface of vesicles.

The variability of the NAAG signal in the assay buffer filtrates from the control conditions and the $KO^{-ATP}$ condition are most likely attributable to experimental or operator error and not the result of NAAG transport. If the changes to the amount of NAAG were the result of transport or incomplete filtration, the loss of NAAG from the assay buffer filtrate would have been accompanied by a proportionate change in the vesicle eluate NAAG content. The reduced NAAG signal within the

assay buffer filtrate and absence from the vesicle eluate of the $KO^{-ATP}$ condition is likely the result of a significant loss of the transport assay solution at some point in the filtration process. The total combined NAAG content of the assay buffer filtrate and vesicle eluate of the $KO^{-ATP}$ condition was therefore much less than the relatively similar NAAG contents of our other conditions and so cannot be compared.

The extremely long filtering times that we encountered while performing this assay were unexpected and had likely significantly affected the outcome of this assay. A likely consequence of the long sample filtering duration is the possibility for equilibration between the vesicles and the assay buffer. Leakage from synaptic vesicles has been previously characterized for glutamate[91-93] as well as GABA[94]. Although NAAG has not been directly demonstrated to leak by similar means, it is reasonable to suspect that after several hours there has likely been significant dissipation of the proton gradient and/or the vesicle NAAG content. Moreover, if vesicles contained no NAAG after the uptake assay, there is also the possibility that NAAG from the assay buffer may have leaked into the vesicles. We therefore cannot draw conclusions regarding the participation of ABCC5 in NAAG transport from this preliminary assay, as we cannot reject the possibility that these results have been significantly skewed due to equilibration. However, after making alterations to the assay protocol to significantly reduce the filtration time, we are confident that equilibration will not have a significant effect.

We also intend to introduce additional assay conditions with specific transporter inhibitors and oxidative phosphorylation uncouplers after this assay has been validated and optimized. Further experiments could include MK-571[70, 71], an ABCC5 inhibitor, and Neu5ac[95], a SLC17A5 inhibitor, to assess the relative contributions of these known NAAG transporters to the loading of vesicles in this transport assay.

We have also begun investigating the feasibility of large-scale expansion culture of the GLUTag or NCI-H716 model L cell lines as an alternative source of *ex vivo* ABCC5-bearing vesicles. Uehara

*et al* have previously used the GLUTag cell line to investigate the corelease of glutamate with GLP-1, which involved the isolation of GLP-1 secretory granules and a vesicle transport assay[40]. The technical challenge in using a cell line instead of model animal tissue is that generating the necessary $10^9$ cells requires adaptation of either our GLUTag or NCI-H716 cell lines for growth in large shaker flasks. The use of a model L cell line as the source of SLMVs for our transport assay would further increase the physiological similarity to L cells *in vivo*.

Due to departmental closures caused by COVID-19, repeating this experiment has not yet been possible. Nonetheless, the validation of a method for obtaining *ex vivo* synaptic vesicles and the proof of feasibility for a transport assay based on NMR substrate detection have established a basis from which to continue investigating the role of ABCC5 in vesicular NAAG transport.

# 6 General Discussion and Conclusion

The capacities of many different ATP-binding cassette transporters to transport a wide variety of substrates has been extensively characterized through broad drug screening and transport assays. However, the function(s) and overall role that many ABC transporters may have within tissues and the body has yet to be fully characterized and may hold much potential. An exciting, new direction for ABC transporters that has arisen in recent years from the discovery that certain ABC transporters act as regulators of signal transduction pathways.

An example of such regulatory behaviour has been demonstrated in ABCC4 (MRP4), another member of the ABCC transporter subfamily with the ability to transport cyclic nucleotides, antiproliferative drugs, and prostaglandins. Mutagenesis screens performed by Jin *et al*[96] in zebrafish found that animals with a mutation in the *abcc4* gene, termed the *leakytail* (*lkt)* mutant, displayed numerous cilia-associated abnormalities. The loss of ABCC4 was confirmed to be a cause of cilia-related pathology in *lkt* mutants by injection of antisense *abcc4* morpholinos, which caused a cilia-associated phenotype that mirrors *lkt* mutants. The *lkt* mutant phenotype could also be rescued by injecting *abcc4* mRNA. Despite considerable overlap of the substrates transported by ABCC transporters, prostaglandin $E_2$ ($PGE_2$) is exclusively transported by ABCC4[97]. The authors therefore hypothesized that the cilia-associated phenotype of *lkt/abcc4* mutants was due to impaired $PGE_2$ signalling caused by a lack of $PGE_2$ export. Supplementation of *lkt* embryo growth media with $PGE_2$ protected against cilia-associated phenotypes and partially restored ciliogenesis, supporting the idea that a lack of free $PGE_2$ contributes to cilia malformation in *lkt/abcc4* mutants. Through both a recombinant cell surface expression model and inside-out membrane vesicle transport assays, the authors reaffirmed that ABCC4 directly transports $PGE_2$ and confirmed the *lkt/abcc4* mutation prevents $PGE_2$ transport. The lack of transport was attributed to a loss of ABCC4 plasma membrane localization and therefore inability to export $PGE_2$. Having shown the relationship between ciliogenesis deficiency and impaired $PGE_2$ export by ABCC4, there remained

the question of how increased amounts of exported $PGE_2$ promotes cilia formation. EP4 is a Gs-protein-coupled receptor (GPCR), which when activated by $PGE_2$ increases intracellular [cAMP] and in turn activates protein kinase A (PKA). The knockdown of EP4 resulted in similar cilia-associated phenotypes as *lkt/abcc4* mutants, which could not be rescued by treatment with $PGE_2$. Administration of forskolin to *ep4*-deficient embryos however was able to partially reverse cilia-related pathology, indicating that $PGE_2$ activates EP4 and the cAMP produced downstream of EP4 promotes ciliogenesis. Finally, anterograde intraflagellar transport (IFT) is a mechanism commonly responsible for the formation of cilia, which may be promoted by cAMP signalling[98]. Treatment of cells with $PGE_2$ was shown to increase the anterograde velocity of IFT proteins, suggesting that $PGE_2$ enhances anterograde IFT and in turn promotes ciliogenesis. The work of Jin *et al*[96] provides robust evidence to demonstrate that ABCC4 regulates ciliogenesis through $PGE_2$ export, which in turn activates the EP4 receptor and promotes anterograde IFT ciliogenesis through cAMP signalling. The comprehensive justification for this conclusion includes the association between ABCC4 expression and normal ciliogenesis, multiple transport assays to confirm $PGE_2$ transport by ABCC4, demonstration of the necessity for EP4 activation by $PGE_2$ and the downstream cAMP it produces, and the acceleration of anterograde IFT by $PGE_2$; the roles of ABCC4, $PGE_2$, EP4, and cAMP outline a complete signalling pathway crucial to ciliogenesis. ABCC4 and the discovery of its role in $PGE_2$-EP4-cAMP-mediated ciliogenesis can serve as a model for investigating other ABC transporters potentially involved in the transport of substrates that influence downstream signalling.

When seeking to investigate the possible roles ABCC5 may play in signalling pathways, it is essential to understand its substrates and transport behaviour. ABCC transporters are also commonly referred to as multidrug-resistance proteins (MRPs), owed largely to initial findings of ABCC1(MRP1) contributing to resistance against a number of anticancer drugs. ABCC transporters generally act as organic anion transporters, varying in affinity to many shared

substrates as well as having unique substrates. It is interesting to note that ABCC1 is also likely capable of cotransporting neutral or basic compounds with glutathione conjugates, which may be an undiscovered behaviour of other ABCC transporters. Due to the initial interest of ABCC transporters in drug resistance and cytotoxicity, the characterization of substrates of ABCC5 was classically performed by overexpression of the transporter in a mammalian cell line. Inside-out membrane vesicles are also often generated from these transfected cells in order to remove possible interference by cytoplasmic substrate metabolism. Using these methods, Jedlitschky *et al*[99] originally found that ABCC5 can mediate the transport of both cGMP and cAMP; transport of cyclic nucleotides by ABCC5 was also sensitive to phosphodiesterase inhibitors. Additional work was performed by Wijnholds *et al*[100] and Reid *et al*[97] to further characterize the affinity of ABCC5 for different nucleotide analogues and the effect of competition between them on transport. Methotrexate (MTX) is another anti-proliferative drug that inhibits the metabolism of folic acid, which had previously been shown the transported by ABCC1-4. Wielinga *et al*[101] using similar techniques demonstrated that ABCC5 transports folic acid as well as a number of antifolate drugs. Interestingly, diglutamylated MTX showed the highest affinity for ABCC5 of the compounds tested, an early indication that ABCC5 may favour the transport of glutamate conjugates. Although the specific affinities for various drugs is of limited use in deciphering the physiological roles of ABCC5, the investigation of both nucleoside analogues and antifolates found that ABCC5 has an apparent low affinity for its endogenous and exogenous substrates. The low affinities of these substrates could suggest either that other ABCC5 substrates remained undiscovered or that ABCC5 functions to protect against or signal the presence of high intracellular concentrations of cyclic nucleotides or folates. Moreover, the differences in substrate affinity between ABCC4 and ABCC5 particularly demonstrated by Reid *et al*[97] indicates that ABCC5 is not redundant to ABCC4 activity and likely possesses unique physiological roles.

Knockdown of ABCC5 in a number of animal models has also been performed to provide insight into potential physiological roles of ABCC5 in tissues and the body. The earliest investigation of *in vivo* ABCC5 knockdown was carried out by Long *et al*[102] in a zebrafish model using dominant-negative suppression of endogenous ABCC5 activity. Impaired ABCC5 activity notably resulted in overall developmental retardation of the body length and pigmentation, with particular reduction eye and head size. The authors also found that intracellular cGMP levels were significantly increased by the inhibition ABCC5 activity but were unchanged by overexpression of ABCC5. This finding agrees with prior *in vitro* observations of a low affinity for cGMP, suggesting ABCC5 has a physiological role of maintaining intracellular cGMP below a certain homeostatic limit but does not further reduce cGMP concentrations.

Work by Shipp *et al*[35, 103] investigated the role of ABCC5 in sea urchin development. Initially the authors found that ABCC5 was highly expressed at the cell membrane of mesodermal pigment cells during gastrulation but did not contribute to differentiation of pigment cells themselves. Knockdown of ABCC5 instead resulted in the prolapse of the gut during gastrulation, indicating that ABCC5 mediates signalling from pigment cells to promote normal gut invagination. Pigment cells are characterized by intracellular cAMP activity, which is a known substrate of ABCC5. Expression of soluble adenylyl cyclase(sAC) was found to be positively correlated with that of ABCC5, and pharmacological inhibition of sAC also resulted in gut prolapse similar to ABCC5 knockdown. Conversely, administration of membrane-permeable cAMP or cGMP prevented gut prolapse in ABCC5 knockdown embryos in a dose-dependent manner. The authors hypothesized from their findings that ABCC5 regulates hindgut invagination by transporting cAMP from pigment cells into the blastula/gastrula cavity to orient the developing gut. This behaviour may not be limited to sea urchin development as ABCC5 is also expressed in the membranes of mammalian amniotic epithelia[104]. This study demonstrated an apparent role for ABCC5 in a cyclic nucleotide

signalling pathway, sharing multiple similarities with ABCC4 in the regulation of signal transduction.

ABCC5 has also been shown to have a physiological role in regulating heme homeostasis in *C. elegans* and zebrafish[105]. A lack of ABCC5 within the intestines of *C. elegans* caused embryonic lethality. Specifically, basolateral expression of ABBC5 by intestinal cells prevented the intracellular accumulation of heme and its analogues. Although not lethal, the knockdown of ABCC5 in zebrafish resulted in severe anaemia, as well as reproduced the developmental retardation shown by Long *et al*[102]. Moreover, expression of ABCC5 in yeast and mammalian cells was positively correlated with heme export, indicating at the least an indirect role in the transport of heme. This study ultimately showed that ABCC5 participates either in the direct transport of heme across the plasma membrane or in regulating the endocytic trafficking of heme from the intestines.

Despite studies of ABCC5 knockdown in metazoan animal models showing a number of distinct pathologies, initial knockout of ABCC5 in mice did not yield any clear phenotype. Work by Jansen *et al*[3] greatly expanded the scope of ABCC5 activity by discovering an *in vivo* role in glutamate-conjugate transport using untargeted metabolomics screens of *Abcc5* KO mice. Various glutamate conjugates and analogues were found to be significantly increased in diverse tissues throughout the body, with accumulation most consistently occurring in the brain; NAAG is the best characterized of these metabolites. Through overexpression of ABCC5 in HEK293 cells as well as inside-out membrane vesicles, NAAG was demonstrated to be directly transported by ABCC5 with an affinity similar to that of the cyclic nucleotides and folates mentioned earlier. ABCC5 has significantly higher levels of expression in the brain and spinal cord compared to other ABCC transporters. ABCC5 is also widely expressed in the brain in contrast to other transporters restricted to a few regions, as seen with ABCC1[106]. Importantly, the transport of glutamate conjugates also appeared to be the primary *in vivo* function of ABCC5 as the metabolomics screening of Jansen *et al*[3] did

not show a similar accumulation of cyclic nucleotides or folates, suggesting a lack of transport may be compensated for by altered metabolism. Given the role of glutamate conjugates in glutamatergic signalling pathways and the expression of ABCC5 in the brain, a regulator role in glutamatergic transmission is the most likely possible function of ABCC5 beyond its established barrier maintenance activity.

Phenotypes resulting from variation in ABCC5 expression have also been found in humans. Direk *et al*[27] performed a candidate gene study on a genomic region including the *ABCC5* gene to investigate the role of the locus in susceptibility to T2DM. An *ABCC5* genetic variant within intron 26 was shown to be genetically associated with T2DM and insulin resistance, with elevated ABCC5 expression in adipose tissue. Moreover, increased ABCC5 expression in non-diabetic individuals, independent of the genetic variant, was associated with reduced peripheral insulin sensitivity and increased visceral fat accumulation. Importantly, the increased T2DM-susceptibility variant of *ABCC5* was determined to be an expression quantitative trait locus, which indicates increased expression is responsible for the increased disease susceptibility. Genome-wide association studies are usually limited to identifying disease-associated SNPs. This study shows that ABCC5-associated pathology may largely arise from altered expression, which can be influenced by non-SNP factors. The genomic screening for possible association of ABCC5 with pathology in humans should certainly be revisited.

Our *Abcc5* knockout mice display subtle yet clear metabolic and neurological phenotypes that would suggest ABCC5 may act as a regulator of signal transduction pathways, similar to ABCC4. In the absence of ABCC5, both male and female KO mice had decreased fat mass and increased sensitivity to insulin compared to wild-type littermates, which is the phenotypic inverse of *ABCC5* overexpression reported in humans. As mentioned in the introduction, GLP-1 release by gut endocrine cells plays a major role in regulating metabolism, which could possibly be affected by ABCC5. Indeed, enteroendocrine cells were shown to express ABCC5 and GLP-1 release was

inversely related to ABCC5 expression, suggesting a causal relationship. Moreover, GLP-1 release was inhibited by addition of exogenous NAAG in both a model gut endocrine cell line and *ex vivo* gut crypts from *Abcc5* KO mice. These findings outlined a possible regulatory pathway, in which ABCC5 transports NAAG into synaptic-like vesicles that can modulate GLP-1 release in a para- or autocrine manner. The experiments shown in this thesis worked towards demonstrating the vesicular localization of ABCC5 in enteroendocrine cells and confirming NAAG is transported by endogenous ABCC5-bearing vesicles. The finding of punctate, intracellular ABCC5 expression is consistent with the notion of regulating glutamatergic activation during exocytosis. Additionally, the vesicular transport assay will allow for crucial *ex vivo* confirmation of NAAG transport, as well as other ABCC5 substrates.

Behavioural testing of our *Abcc5* KO mice found additional differences from their wildtype counterparts. Assessment of the acoustic startle response of *Abcc5* KO mice showed impairment of prepulse inhibition (PPI), in which a smaller "prepulse" tone normally attenuates a mouse' response to a large acoustic pulse; loss of PPI is considered to be an effective biomarker for schizophrenia. Intriguingly, this data is in contrast to the negative outcome of a different schizophrenia test reported but unpublished by Jansen *et al*[3], who used the phencyclidine-induced locomotor activity assay. The phencyclidine is an inhibitor of the NMDAR that induces schizophrenia symptoms, and reduction of the response to phencyclidine suggests an experimental animal is already in at least a partial schizophrenic state. A prior study[107] had found that increased synaptic NAAG levels caused by inhibiting its enzymatic breakdown by NAAG peptidase had reduced the hyperlocomotion effect of phencyclidine, suggesting that the NMDAR was already partially antagonized by elevated NAAG in the synaptic cleft. In the case of *Abcc5* KO mice, the phencyclidine-induced locomotor activity assay was likely inappropriate. We hypothesize that the increase in NAAG levels measured in the brains of *Abcc5* KO mice were most likely a result of NAAG being confined within neurons, unable to be released and metabolised by NAAG peptidase

in the synaptic cleft. Additionally, our *Abcc5* KO mice did show increased overall activity, whereas the method used by Jansen *et al*[3] did not, which may have affected their conclusions regarding hyperlocomotion.

The schizophrenic phenotype suggested by our PPI test results was unexpected given the predominance of literature suggesting that NAAG within the synaptic cleft positively correlates with symptoms of schizophrenia. Possible explanations could include, but are not limited to, a reduction in the synaptic glutamate content caused by trapping of glutamate within intracellular NAAG or an inhibition of pyramidal neurons as a result of increased NMDAR activity on GABAergic interneurons. Regardless of the mechanism responsible, ABCC5 is somehow involved in glutamatergic signalling in the brain to the extent that behaviour is modified by a lack of ABCC5 activity. The isolation of ABCC5+ synaptic vesicles from mouse brains shown in this thesis furthers the notion that ABCC5 participates in synaptic transmission. If our vesicular transport assay demonstrates direct NAAG transport by ABCC5, we could more confidently hypothesize that ABCC5 functions to load NAAG into synaptic vesicles that regulate glutamatergic signalling at pre- and post-synaptic neurons. An exciting possibility is that the location and intensity of ABCC5 expression may act as an upstream regulator of the contribution of NAAG to glutamatergic signalling. Although ABCC5 deficiency in humans has not yet been characterized, variation in ABCC5 expression levels have already been shown to produce a clear metabolic phenotype by Direk *et al*[27] and there is preliminary evidence for a similar expression-based association with schizophrenia[108].

Both of our investigations into the metabolic and neurological phenotypes of *Abcc5* KO mice suggest altered contribution of NAAG in glutamatergic signalling. However, there remains considerable uncertainty regarding NAAG in synaptic transmission. NAAG has been reported in glutamatergic, GABAergic, cholinergic, and noradrenergic neuronal systems, and behaviour between different systems is unclear. The NMDAR is an excitatory ion channel opened by binding

of glutamate and glycine. NAAG was found to specifically bind to NMDAR and have a weak agonistic effect. However, several other studies showed NAAG to antagonize the activity of NMDAR. Together these findings would suggest NAAG may act as an inverse agonist, increasing or decreasing NMDAR activity likely depending on the prevailing signalling activity of glutamate in the synaptic cleft. Additionally, NAAG is catabolized by the enzyme NAAG peptidase, also called glutamate carboxypeptidase type II (GCPII), into *N*-acetylaspartate and glutamate, of which the latter is capable of activating NMDAR. The circumstances that determine whether NAAG overall acts as an agonist or antagonist of NMDAR remain unclear. The other major component of NAAG signalling is the inhibitory, metabotropic glutamate receptor mGluR3, at which NAAG has been clearly demonstrated to act as a full agonist. mGluR3 is predominantly expressed presynaptically and activation inhibits neurotransmitter release from presynaptic neurons. Combining the ability of NAAG to inhibit presynaptic glutamate release as well as the select reports of NMDAR antagonism, NAAG is predominantly considered to be an antagonist of glutamatergic signalling.

While the cause of schizophrenia is likely multifactorial, there is substantial pharmacological evidence to suggest that hypofunction of NMDAR can produce symptoms and behaviour typical of schizophrenia. NMDAR in the context schizophrenia is primarily studied using the antagonist phencyclidine. Although there remains uncertainty regarding the interaction of NAAG and NMDAR, there is ample genetic and pharmacological evidence that associates the loss of NAAG peptidase/GCPII activity and increased levels of NAAG with a schizophrenic phenotype. However, it is important to note that these studies caused global losses of NAAG peptidase/GCPII and the role of NAAG may be different between brain regions or neural systems. NAAG appears to be protective against excess of glutamatergic signalling by antagonism of NMDAR and presynaptic glutamate release, but high, unregulated amounts of NAAG can contribute to schizophrenia[109]. However, although schizophrenia is commonly attributed reduced glutamate signalling, there are

also a few reports of increased NAAG reducing schizophrenic symptoms. Our findings in *Abcc5* KO mice could be another such example. Further investigation into the role ABCC5 plays in glutamatergic signalling via NAAG should clarify the effect of NAAG specifically at the NMDAR and generally in the synaptic cleft within the brain regions and neural systems expressing ABCC5.

As a final note on NAAG signalling and possible areas where ABCC5 may regulate NAAG transport and downstream physiology, NAAG peptidase/GCP2 is also commonly referred to as prostate specific membrane antigen (PSMA). GCP2/PSMA is highly upregulated in cancer of the prostate as well as others. Additionally, Nguyen *et al*[110] recently demonstrated that NAAG is highly concentrated within several cancers and increased with higher severity of the cancer. NAAG appears to act as a reservoir for storing glutamate to promote growth when glutamate production is reduced, upon which cancer metabolism has been found to heavily rely[111-113]. Intriguingly, ABCC5 is also highly upregulated in both prostate cancer and gliomas[114-116], which are associated with reliance on NAAG as a glutamate reservoir. These findings together with our work and the literature surrounding ABCC5 and NAAG suggest ABCC5 may also have a role regulating tumour growth via NAAG-glutamate reservoirs.

Ultimately, both the metabolic and neurological phenotypes of *Abcc5* knockout mice can potentially be attributed to changes in the efficacy of glutamatergic signalling where ABCC5 is expressed. Work is ongoing in our lab to elucidate the underlying mechanisms by which ABCC5 interacts with glutamatergic signalling in both the gut and the brain, either through direct action by its substrates or influence on downstream signalling. This thesis worked to show that ABCC5 can be expressed intracellularly in enteroendocrine cells and to develop a vesicular transport assay to assess whether ABCC5 is capable of loading NAAG into synaptic-like microvesicles. Demonstrating potential regulatory behaviour for ABCC5 in the gut and brain would greatly expand the possible roles that ABC transporters serve in physiology. Characterizing the regulatory

role of ABCC5 in the relatively simple model of gut endocrine cells also would be invaluable for uncovering the potential role this transporter plays in neurons and the brain.

**Future Directions**

Numerous experiments have been suggested within this thesis to further explore ABCC5 expression and its possible functions, which are summarised briefly. Further attempts to colocalize ABCC5 with markers of intracellular vesicle pools would aid in determining whether ABCC5 participates in substrate sequestration, exocytotic signalling following stimulation, or both when expressed intracellularly. The FDA staining can be utilized for *ex vivo* histological staining to identify cells that express ABCC5 at the cell membrane. Additionally, if validated to be specifically accumulated within ABCC5+ vesicles, FDA could be used to investigate the abundance and behaviour of these vesicles *in vivo*. The two protein bands observed when performing western blots for ABCC5 should be further investigated to determine their origins. Additional western blots comparing tissue known to express ABCC5 on the cell membrane, our NCI-H716 or GLUTag model L cell lines with intracellular ABCC5, and the subcellular fractions from vesicle isolation would allow for attribution of where these bands are expressed. Moving forward, it will be important to investigate the cause and possible consequences of these different forms of ABCC5. Finally, the vesicular transport assay must be repeated with the outlined improvements to assess whether ABCC5 has a role in the vesicular loading of NAAG, or other substrates such as cAMP and cGMP.

The primary goal of this thesis was to investigate the expression and possible vesicular function of ABCC5. The results obtained from these experiments strongly suggest an intracellular, vesicular role for ABCC5 in enteroendocrine cells, as well as outline novel protocols for further investigating the specific functions of ABCC5. There remains considerable uncertainty regarding the underlying mechanisms of how ABCC5 influences metabolism and the brain. Our evidence thus far strongly

points towards some degree of participation in glutamatergic signalling; ABCC5 may act as a regulator of signal transduction pathways, which is a largely unexplored possibility for ABC transporters.

## References


1. Dean, M., A. Rzhetsky, and R. Allikmets, *The human ATP-binding cassette (ABC) transporter superfamily.* Genome Res, 2001. **11**(7): p. 1156-66.
2. Sodani, K., et al., *Multidrug resistance associated proteins in multidrug resistance.* Chinese journal of cancer, 2012. **31**(2): p. 58-72.
3. Jansen, R.S., et al., *ATP-binding Cassette Subfamily C Member 5 (ABCC5) Functions as an Efflux Transporter of Glutamate Conjugates and Analogs.* J Biol Chem, 2015. **290**(51): p. 30429-40.
4. Puttfarcken, P.S., et al., *N-acetyl-aspartylglutamate modulation of N-methyl-D-aspartate-stimulated [3H]norepinephrine release from rat hippocampal slices.* J Pharmacol Exp Ther, 1993. **266**(2): p. 796-803.
5. Wroblewska, B., et al., *N-acetylaspartylglutamate selectively activates mGluR3 receptors in transfected cells.* J Neurochem, 1997. **69**(1): p. 174-81.
6. Neale, J.H., et al., *Advances in understanding the peptide neurotransmitter NAAG and appearance of a new member of the NAAG neuropeptide family.* J Neurochem, 2011. **118**(4): p. 490-8.
7. Boland, B.B., C.J. Rhodes, and J.S. Grimsby, *The dynamic plasticity of insulin production in β-cells.* Molecular Metabolism, 2017. **6**(9): p. 958-973.
8. Shoelson, S.E., J. Lee, and A.B. Goldfine, *Inflammation and insulin resistance.* The Journal of clinical investigation, 2006. **116**(7): p. 1793-1801.
9. Kahn, S.E., et al., *Quantification of the Relationship Between Insulin Sensitivity and β-Cell Function in Human Subjects: Evidence for a Hyperbolic Function.* Diabetes, 1993. **42**(11): p. 1663-1672.
10. Kahn, S.E., *The Importance of β-Cell Failure in the Development and Progression of Type 2 Diabetes.* The Journal of Clinical Endocrinology & Metabolism, 2001. **86**(9): p. 4047-4058.
11. Butler, A.E., et al., *β-Cell Deficit and Increased β-Cell Apoptosis in Humans With Type 2 Diabetes.* Diabetes, 2003. **52**(1): p. 102-110.
12. Røder, M.E., et al., *Disproportionately Elevated Proinsulin Levels Reflect the Degree of Impaired B Cell Secretory Capacity in Patients with Noninsulin-Dependent Diabetes Mellitus1.* The Journal of Clinical Endocrinology & Metabolism, 1998. **83**(2): p. 604-608.
13. Rosengren, A.H., et al., *Reduced insulin exocytosis in human pancreatic β-cells with gene variants linked to type 2 diabetes.* Diabetes, 2012. **61**(7): p. 1726-1733.
14. SAKO, Y. and V.E. GRILL, *A 48-hour Lipid Infusion in the Rat Time-Dependently Inhibits Glucose-Induced Insulin Secretion and B Cell Oxidation Through a Process Likely Coupled to Fatty Acid Oxidation*.* Endocrinology, 1990. **127**(4): p. 1580-1589.
15. Zhou, Y.P. and V.E. Grill, *Long-term exposure of rat pancreatic islets to fatty acids inhibits glucose-induced insulin secretion and biosynthesis through a glucose fatty acid cycle.* The Journal of clinical investigation, 1994. **93**(2): p. 870-876.
16. Drucker, D.J., *The biology of incretin hormones.* Cell Metabolism, 2006. **3**(3): p. 153-165.
17. Verdich, C., et al., *The role of postprandial releases of insulin and incretin hormones in meal-induced satiety - Effect of obesity and weight reduction.* International journal of obesity and related metabolic disorders : journal of the International Association for the Study of Obesity, 2001. **25**: p. 1206-14.
18. Cho, Y.M., Y. Fujita, and T.J. Kieffer, *Glucagon-Like Peptide-1: Glucose Homeostasis and Beyond.* Annual Review of Physiology, 2014. **76**(1): p. 535-559.
19. Nauck, M.A., et al., *Glucagon-like peptide 1 inhibition of gastric emptying outweighs its insulinotropic effects in healthy humans.* American Journal of Physiology-Endocrinology and Metabolism, 1997. **273**(5): p. E981-E988.

20. Willms, B., et al., *Gastric emptying, glucose responses, and insulin secretion after a liquid test meal: effects of exogenous glucagon-like peptide-1 (GLP-1)-(7-36) amide in type 2 (noninsulin-dependent) diabetic patients.* The Journal of Clinical Endocrinology & Metabolism, 1996. **81**(1): p. 327-332.
21. Nauck, M., *Incretin therapies: highlighting common features and differences in the modes of action of glucagon-like peptide-1 receptor agonists and dipeptidyl peptidase-4 inhibitors.* Diabetes, obesity & metabolism, 2016. **18**(3): p. 203-216.
22. Hutch, C.R. and D. Sandoval, *The Role of GLP-1 in the Metabolic Success of Bariatric Surgery.* Endocrinology, 2017. **158**(12): p. 4139-4151.
23. Bray, G.A., et al., *Management of obesity.* The Lancet, 2016. **387**(10031): p. 1947-1956.
24. Jirapinyo, P., et al., *A Meta-Analysis of GLP-1 After Roux-En-Y Gastric Bypass: Impact of Surgical Technique and Measurement Strategy.* Obes Surg, 2018. **28**(3): p. 615-626.
25. ten Kulve, J.S., et al., *Elevated Postoperative Endogenous GLP-1 Levels Mediate Effects of Roux-en-Y Gastric Bypass on Neural Responsivity to Food Cues.* Diabetes Care, 2017. **40**(11): p. 1522-1529.
26. Hansen, C.F., et al., *Hypertrophy dependent doubling of L-cells in Roux-en-Y gastric bypass operated rats.* PloS one, 2013. **8**(6): p. e65696-e65696.
27. Direk, K., et al., *ABCC5 transporter is a novel type 2 diabetes susceptibility gene in European and African American populations.* Ann Hum Genet, 2014. **78**(5): p. 333-44.
28. Pais, R., et al., *Angiotensin II Type 1 Receptor-Dependent GLP-1 and PYY Secretion in Mice and Humans.* Endocrinology, 2016. **157**(10): p. 3821-3831.
29. Cyranka, M., et al., *Abcc5 Knockout Mice Have Lower Fat Mass and Increased Levels of Circulating GLP-1.* Obesity (Silver Spring, Md.), 2019. **27**(8): p. 1292-1304.
30. Kuhre, R.E., et al., *Peptide production and secretion in GLUTag, NCI-H716, and STC-1 cells: a comparison to native L-cells.* J Mol Endocrinol, 2016. **56**(3): p. 201-11.
31. Reimann, F., et al., *Glutamine potently stimulates glucagon-like peptide-1 secretion from GLUTag cells.* Diabetologia, 2004. **47**(9): p. 1592-601.
32. Mena, A., et al., *Reduced Prepulse Inhibition as a Biomarker of Schizophrenia.* Frontiers in Behavioral Neuroscience, 2016. **10**(202).
33. Bergeron, R. and J.T. Coyle, *NAAG, NMDA receptor and psychosis.* Current medicinal chemistry, 2012. **19**(9): p. 1360-1364.
34. Koehn, L., *ABC efflux transporters at blood-central nervous system barriers and their implications for treating spinal cord disorders.* Neural Regeneration Research, 2020. **15**(7): p. 1235-1242.
35. Shipp, L.E. and A. Hamdoun, *ATP-binding cassette (ABC) transporter expression and localization in sea urchin development.* Developmental dynamics : an official publication of the American Association of Anatomists, 2012. **241**(6): p. 1111-1124.
36. Kavishe, R.A., et al., *Localization of the ATP-binding cassette (ABC) transport proteins PfMRP1, PfMRP2, and PfMDR5 at the Plasmodium falciparum plasma membrane.* Malaria journal, 2009. **8**: p. 205-205.
37. Psichas, A., et al., *Mixed Primary Cultures of Murine Small Intestine Intended for the Study of Gut Hormone Secretion and Live Cell Imaging of Enteroendocrine Cells.* J Vis Exp, 2017(122).
38. Ahmed, S., et al., *Small-scale isolation of synaptic vesicles from mammalian brain.* Nature Protocols, 2013. **8**: p. 998.
39. Hell, J.W., et al., *Uptake of GABA by rat brain synaptic vesicles isolated by a new procedure.* The EMBO journal, 1988. **7**(10): p. 3023-3029.
40. Uehara, S., et al., *Vesicular storage and secretion of L-glutamate from glucagon-like peptide 1-secreting clonal intestinal L cells.* J Neurochem, 2006. **96**(2): p. 550-60.

41. Zimmermann, J., M.A. Herman, and C. Rosenmund, *Co-release of glutamate and GABA from single vesicles in GABAergic neurons exogenously expressing VGLUT3.* Frontiers in synaptic neuroscience, 2015. **7**: p. 16-16.
42. Klijn, C., et al., *A comprehensive transcriptional portrait of human cancer cell lines.* Nature Biotechnology, 2015. **33**(3): p. 306-312.
43. Fremeau, R.T., Jr., et al., *VGLUTs define subsets of excitatory neurons and suggest novel roles for glutamate.* Trends in Neurosciences, 2004. **27**(2): p. 98-103.
44. Li, T., F.-K. Ghishan, and L. Bai, *Molecular physiology of vesicular glutamate transporters in the digestive system.* World journal of gastroenterology, 2005. **11**(12): p. 1731-1736.
45. Calhoun, M.E., et al., *Comparative evaluation of synaptophysin-based methods for quantification of synapses.* Journal of neurocytology, 1996. **25**(12): p. 821-828.
46. Chapuy, B., et al., *Intracellular ABC transporter A3 confers multidrug resistance in leukemia cells by lysosomal drug sequestration.* Leukemia, 2008. **22**(8): p. 1576-1586.
47. Huynh, K.K., et al., *LAMP proteins are required for fusion of lysosomes with phagosomes.* The EMBO journal, 2007. **26**(2): p. 313-324.
48. Kim, S.-W., J. Roh, and C.-S. Park, *Immunohistochemistry for Pathologists: Protocols, Pitfalls, and Tips.* Journal of pathology and translational medicine, 2016. **50**(6): p. 411-418.
49. Burry, R.W., *Immunocytochemistry: a practical guide for biomedical research*. 2010, New York: Springer. 223.
50. Dabbs, D.J., *Diagnostic immunohistochemistry: theranostic and genomic application.* NY: Saunders Elsevier, 2010.
51. Burry, R.W., *Controls for immunocytochemistry: an update.* The journal of histochemistry and cytochemistry : official journal of the Histochemistry Society, 2011. **59**(1): p. 6-12.
52. St. Croix, C.M., S.H. Shand, and S.C. Watkins, *Confocal microscopy: comparisons, applications, and problems.* BioTechniques, 2005. **39**(6S): p. S2-S5.
53. Turner, J.N., et al., *Three-dimensional imaging and image analysis of hippocampal neurons: Confocal and digitally enhanced wide field microscopy.* Microscopy Research and Technique, 1994. **29**(4): p. 269-278.
54. Jonkman, J. and C.M. Brown, *Any Way You Slice It-A Comparison of Confocal Microscopy Techniques.* Journal of biomolecular techniques : JBT, 2015. **26**(2): p. 54-65.
55. North, A.J., *Seeing is believing? A beginners' guide to practical pitfalls in image acquisition.* The Journal of cell biology, 2006. **172**(1): p. 9-18.
56. Swedlow, J.R. and M. Platani, *Live cell imaging using wide-field microscopy and deconvolution.* Cell Struct Funct, 2002. **27**(5): p. 335-41.
57. Zhang, Y., et al., *Plasma Membrane Localization of Multidrug Resistance-Associated Protein Homologs in Brain Capillary Endothelial Cells.* Journal of Pharmacology and Experimental Therapeutics, 2004. **311**(2): p. 449.
58. Nies, A.T., et al., *Expression and immunolocalization of the multidrug resistance proteins, MRP1-MRP6 (ABCC1-ABCC6), in human brain.* Neuroscience, 2004. **129**(2): p. 349-60.
59. Borst, P., C. de Wolf, and K. van de Wetering, *Multidrug resistance-associated proteins 3, 4, and 5.* Pflügers Archiv - European Journal of Physiology, 2007. **453**(5): p. 661-673.
60. Soontornmalai, A., M.L.H. Vlaming, and J.M. Fritschy, *Differential, strain-specific cellular and subcellular distribution of multidrug transporters in murine choroid plexus and blood–brain barrier.* Neuroscience, 2006. **138**(1): p. 159-169.
61. Fletcher, J.I., et al., *ABC transporters in cancer: more than just drug efflux pumps.* Nature Reviews Cancer, 2010. **10**(2): p. 147-156.
62. Morris, M.E., V. Rodriguez-Cruz, and M.A. Felmlee, *SLC and ABC Transporters: Expression, Localization, and Species Differences at the Blood-Brain and the Blood-Cerebrospinal Fluid Barriers.* Aaps j, 2017. **19**(5): p. 1317-1331.

63. Herget, M. and R. Tampé, *Intracellular peptide transporters in human--compartmentalization of the "peptidome".* Pflugers Arch, 2007. **453**(5): p. 591-600.
64. Proffitt, R.T., J.V. Tran, and P. Reynolds, *A fluorescence digital image microscopy system for quantifying relative cell numbers in tissue culture plates.* Cytometry, 1996. **24**(3): p. 204-213.
65. Boender, J., *Fluorescein-diacetate, a fluorescent dye compound stain for rapid evaluation of the viability of mammalian oocytes prior to in vitro studies.* Veterinary Quarterly, 1984. **6**(4): p. 236-240.
66. McAleer, M.A., et al., *pABC11 (Also Known as MOAT-C and MRP5), a Member of the ABC Family of Proteins, Has Anion Transporter Activity but Does Not Confer Multidrug Resistance When Overexpressed in Human Embryonic Kidney 293 Cells.* Journal of Biological Chemistry, 1999. **274**(33): p. 23541-23548.
67. *The molecular probes handbook: a guide to fluorescent probes and labeling technologies*. 11. ed ed. 2010, Carlsbad, Calif.: Life Technologies. 1060.
68. Franco, R. and L. Zavala-Flores, *ABCC Transporters*, in *Encyclopedia of Cancer*, M. Schwab, Editor. 2016, Springer Berlin Heidelberg: Berlin, Heidelberg. p. 1-5.
69. Evers, R., et al., *Drug export activity of the human canalicular multispecific organic anion transporter in polarized kidney MDCK cells expressing cMOAT (MRP2) cDNA.* The Journal of Clinical Investigation, 1998. **101**(7): p. 1310-1319.
70. Bertollotto, G.M., et al., *Inhibition of Multidrug Resistance Proteins by MK 571 Enhances Bladder, Prostate, and Urethra Relaxation through cAMP or cGMP Accumulation.* Journal of Pharmacology and Experimental Therapeutics, 2018. **367**(1): p. 138.
71. Sager, G., et al., *Novel cGMP efflux inhibitors identified by virtual ligand screening (VLS) and confirmed by experimental studies.* Journal of medicinal chemistry, 2012. **55**(7): p. 3049-3057.
72. Asokan, A. and M.J. Cho, *Exploitation of Intracellular pH Gradients in the Cellular Delivery of Macromolecules.* Journal of Pharmaceutical Sciences, 2002. **91**(4): p. 903-913.
73. Demaurex, N., *pH Homeostasis of Cellular Organelles.* Physiology, 2002. **17**(1): p. 1-5.
74. Lebedeva, I.V., P. Pande, and W.F. Patton, *Sensitive and Specific Fluorescent Probes for Functional Analysis of the Three Major Types of Mammalian ABC Transporters.* PLOS ONE, 2011. **6**(7): p. e22429.
75. *Membrane transport: a practical approach*. The practical approach series. 2000, Oxford ; New York: Oxford University Press. 320.
76. Hnasko, T.S. and R.H. Edwards, *Neurotransmitter corelease: mechanism and physiological role.* Annu Rev Physiol, 2012. **74**: p. 225-43.
77. Chao, Y. and D. Fu, *Kinetic study of the antiport mechanism of an Escherichia coli zinc transporter, ZitB.* J Biol Chem, 2004. **279**(13): p. 12043-50.
78. Marion, D., *An introduction to biological NMR spectroscopy.* Molecular & cellular proteomics : MCP, 2013. **12**(11): p. 3006-3025.
79. Stothers, J.B., *13C NMR Spectroscopy: A Brief Review.* Applied Spectroscopy, 1972. **26**(1): p. 1-16.
80. Günther, H., *NMR Spectroscopy: Basic Principles, Concepts and Applications in Chemistry*. 2013: Wiley.
81. Rodrigues, T.B., J. Valette, and A.-K. Bouzier-Sore, *(13)C NMR spectroscopy applications to brain energy metabolism.* Frontiers in neuroenergetics, 2013. **5**: p. 9-9.
82. Hoffman, R.A., *Analysis of nmr spectra*. 2012, Place of publication not identified: Springer-Verlag Berlin An.
83. Wong, K.C., *Review of NMR Spectroscopy: Basic Principles, Concepts and Applications in Chemistry.* Journal of Chemical Education, 2014. **91**(8): p. 1103-1104.

84. Richards, P., et al., *High fat diet impairs the function of glucagon-like peptide-1 producing L-cells.* Peptides, 2016. **77**: p. 21-27.
85. Stojic, J., H. Stöhr, and B.H.F. Weber, *Three novel ABCC5 splice variants in human retina and their role as regulators of ABCC5 gene expression.* BMC molecular biology, 2007. **8**: p. 42-42.
86. Zhou, H., et al., *Toward a Comprehensive Characterization of a Human Cancer Cell Phosphoproteome.* Journal of Proteome Research, 2013. **12**(1): p. 260-271.
87. Olsen, J.V., et al., *Quantitative Phosphoproteomics Reveals Widespread Full Phosphorylation Site Occupancy During Mitosis.* Science Signaling, 2010. **3**(104): p. ra3.
88. Nishiye, H., et al., *A new method for electron microscopic observation of isolated synaptic vesicles labelled with monoclonal antibody.* Neurosci Res, 1988. **5**(6): p. 567-76.
89. Groenborg, M., et al., *Proteome analysis of synaptic vesicles.* Proteomic of the nervous system, 141-165 (2008), 2020.
90. Moriyama, Y. and N. Nelson, *Cold inactivation of vacuolar proton-ATPases.* J Biol Chem, 1989. **264**(6): p. 3577-82.
91. Carlson, M.D. and T. Ueda, *Accumulated glutamate levels in the synaptic vesicle are not maintained in the absence of active transport.* Neuroscience letters, 1990. **110**(3): p. 325-330.
92. Maycox, P.R., T. Deckwerth, and R. Jahn, *Bacteriorhodopsin drives the glutamate transporter of synaptic vesicles after co-reconstitution.* The EMBO journal, 1990. **9**(5): p. 1465-1469.
93. Parsons, R.L., et al., *Empty synaptic vesicles recycle and undergo exocytosis at vesamicol-treated motor nerve terminals.* J Neurophysiol, 1999. **81**(6): p. 2696-700.
94. Takami, C., et al., *Impact of vesicular glutamate leakage on synaptic transmission at the calyx of Held.* The Journal of physiology, 2017. **595**(4): p. 1263-1271.
95. Lodder-Gadaczek, J., V. Gieselmann, and M. Eckhardt, *Vesicular uptake of N-acetylaspartylglutamate is catalysed by sialin (SLC17A5).* Biochem J, 2013. **454**(1): p. 31-8.
96. Jin, D., et al., *Prostaglandin signalling regulates ciliogenesis by modulating intraflagellar transport.* Nat Cell Biol, 2014. **16**(9): p. 841-51.
97. Reid, G., et al., *The human multidrug resistance protein MRP4 functions as a prostaglandin efflux transporter and is inhibited by nonsteroidal antiinflammatory drugs.* Proc Natl Acad Sci U S A, 2003. **100**(16): p. 9244-9.
98. Besschetnova, T.Y., et al., *Identification of signaling pathways regulating primary cilium length and flow-mediated adaptation.* Curr Biol, 2010. **20**(2): p. 182-7.
99. Jedlitschky, G., B. Burchell, and D. Keppler, *The Multidrug Resistance Protein 5 Functions as an ATP-dependent Export Pump for Cyclic Nucleotides.* The Journal of biological chemistry, 2000. **275**: p. 30069-74.
100. Wijnholds, J., et al., *Multidrug-resistance protein 5 is a multispecific organic anion transporter able to transport nucleotide analogs.* Proc Natl Acad Sci U S A, 2000. **97**(13): p. 7476-81.
101. Wielinga, P., et al., *The Human Multidrug Resistance Protein MRP5 Transports Folates and Can Mediate Cellular Resistance against Antifolates.* Cancer Research, 2005. **65**(10): p. 4425.
102. Long, Y., et al., *Molecular analysis, developmental function and heavy metal-induced expression of ABCC5 in zebrafish.* Comp Biochem Physiol B Biochem Mol Biol, 2011. **158**(1): p. 46-55.
103. Shipp, L.E., et al., *ABCC5 is required for cAMP-mediated hindgut invagination in sea urchin embryos.* Development, 2015. **142**(20): p. 3537.
104. Aye, I.L., et al., *Expression, localisation and activity of ATP binding cassette (ABC) family of drug transporters in human amnion membranes.* Placenta, 2007. **28**(8-9): p. 868-77.
105. Korolnek, T., et al., *Control of metazoan heme homeostasis by a conserved multidrug resistance protein.* Cell metabolism, 2014. **19**(6): p. 1008-1019.

106. Rao, V.V., et al., *Choroid plexus epithelial expression of MDR1 P glycoprotein and multidrug resistance-associated protein contribute to the blood-cerebrospinal-fluid drug-permeability barrier.* Proc Natl Acad Sci U S A, 1999. **96**(7): p. 3900-5.
107. Zuo, D., et al., *Effects of N-acetylaspartylglutamate (NAAG) peptidase inhibition on release of glutamate and dopamine in prefrontal cortex and nucleus accumbens in phencyclidine model of schizophrenia.* J Biol Chem, 2012. **287**(26): p. 21773-82.
108. *GTEx Portal.*
109. Evans, J.C., et al., *The therapeutic and diagnostic potential of the prostate specific membrane antigen/glutamate carboxypeptidase II (PSMA/GCPII) in cancer and neurological disease.* British journal of pharmacology, 2016. **173**(21): p. 3041-3079.
110. Nguyen, T., et al., *Uncovering the Role of N-Acetyl-Aspartyl-Glutamate as a Glutamate Reservoir in Cancer.* Cell Rep, 2019. **27**(2): p. 491-501.e6.
111. Harding, J.J., et al., *Safety and tolerability of increasing doses of CB-839, a first-in-class, orally administered small molecule inhibitor of glutaminase, in solid tumors*. 2015, American Society of Clinical Oncology.
112. Tanaka, K., et al., *Compensatory glutamine metabolism promotes glioblastoma resistance to mTOR inhibitor treatment.* The Journal of clinical investigation, 2015. **125**(4): p. 1591-1602.
113. Son, J., et al., *Glutamine supports pancreatic cancer growth through a KRAS-regulated metabolic pathway.* Nature, 2013. **496**(7443): p. 101-5.
114. Zhang, H., et al., *Loss of miR-516a-3p mediates upregulation of ABCC5 in prostate cancer and drives its progression.* OncoTargets and therapy, 2018. **11**: p. 3853-3867.
115. Wang, Z., et al., *Targeting miR-381-NEFL axis sensitizes glioblastoma cells to temozolomide by regulating stemness factors and multidrug resistance factors.* Oncotarget, 2015. **6**(5): p. 3147-3164.
116. Jeon, H.M., et al., *ID4 imparts chemoresistance and cancer stemness to glioma cells by derepressing miR-9*-mediated suppression of SOX2.* Cancer Res, 2011. **71**(9): p. 3410-21.